NAVAL POSTGRADUATE SCHOOL

MONTEREY, CALIFORNIA

THESIS

EVOLUTION OF THE ELECTRON BEAM ENVELOPE IN A FREE ELECTRON LASER BEAMLINE

by

Nainn-Tzuu Shen

December 2013

Thesis Advisor: Joseph Blau
Co-Advisor: William Colson

Approved for public release; distribution is unlimited

Reissued 27 Aug 2019 with corrected SF298.

THIS PAGE INTENTIONALLY LEFT BLANK

REPORT DOCUMENTATION PAGE			Form Approved OMB No. 0704–0188
Public reporting burden for this collection of information is estimated to average 1 hour per response, including the time for reviewing instruction, searching existing data sources, gathering and maintaining the data needed, and completing and reviewing the collection of information. Send comments regarding this burden estimate or any other aspect of this collection of information, including suggestions for reducing this burden, to Washington headquarters Services, Directorate for Information Operations and Reports, 1215 Jefferson Davis Highway, Suite 1204, Arlington, VA 22202–4302, and to the Office of Management and Budget, Paperwork Reduction Project (0704–0188) Washington, DC 20503.			
1. AGENCY USE ONLY ***(Leave blank)***	**2. REPORT DATE** December 2013	**3. REPORT TYPE AND DATES COVERED** Master's Thesis	
4. TITLE AND SUBTITLE EVOLUTION OF THE ELECTRON BEAM ENVELOPE IN A FREE ELECTRON LASER BEAMLINE		**5. FUNDING NUMBERS**	
6. AUTHOR(S) Nainn-Tzuu Shen			
7. PERFORMING ORGANIZATION NAME(S) AND ADDRESS(ES) Naval Postgraduate School Monterey, CA 93943–5000		**8. PERFORMING ORGANIZATION REPORT NUMBER**	
9. SPONSORING /MONITORING AGENCY NAME(S) AND ADDRESS(ES) N/A		**10. SPONSORING/MONITORING AGENCY REPORT NUMBER**	
11. SUPPLEMENTARY NOTES The views expressed in this thesis are those of the author and do not reflect the official policy or position of the Department of Defense or the U.S. Government. IRB Protocol number ____N/A____.			
12a. DISTRIBUTION / AVAILABILITY STATEMENT Approved for public release; distribution is unlimited		**12b. DISTRIBUTION CODE** A	

13. ABSTRACT (maximum 200 words)

The free electron laser (FEL) is a new generation of laser whose development motivates further research in basic and applied physics. Unlike a conventional laser that uses a gas or solid state gain medium, the FEL gain medium is a relativistic electron beam produced by a particle accelerator. This thesis will explore electron beam dynamics in an FEL, including the beam envelope equation, which will help us understand the evolution of electron betatron motion in the undulator. Dipole magnets, quadrupoles, and solenoids play important roles in transporting and focusing in an FEL beamline. The dipole magnets redirect the electron beam to a beam dump or recirculate the electrons for energy recovery. The quadrupoles and solenoids collimate and focus the electron beam. Simulations and theory are used to model and study a simple FEL beamline.

14. SUBJECT TERMS free electron laser beamline, betatron motion, beam envelope, quadrupole focusing, solenoid focusing, and bending magnet			**15. NUMBER OF PAGES** 73
			16. PRICE CODE
17. SECURITY CLASSIFICATION OF REPORT Unclassified	**18. SECURITY CLASSIFICATION OF THIS PAGE** Unclassified	**19. SECURITY CLASSIFICATION OF ABSTRACT** Unclassified	**20. LIMITATION OF ABSTRACT** UU

NSN 7540–01–280–5500 Standard Form 298 (Rev. 2–89)
Prescribed by ANSI Std. 239–18

THIS PAGE INTENTIONALLY LEFT BLANK

Approved for public release; distribution is unlimited

EVOLUTION OF THE ELECTRON BEAM ENVELOPE IN A FREE ELECTRON LASER BEAMLINE

Nainn-Tzuu Shen
Lieutenant Commander, Taiwan Navy
B.S., Taiwan Naval Academy, 1999

Submitted in partial fulfillment of the
requirements for the degree of

MASTER OF SCIENCE IN APPLIED PHYSICS

from the

NAVAL POSTGRADUATE SCHOOL
December 2013

Author: Nainn-Tzuu Shen

Approved by: Joseph Blau
Thesis Advisor

William Colson
Co-Advisor

Andres Larraza
Chair, Department of Physics

THIS PAGE INTENTIONALLY LEFT BLANK

ABSTRACT

The free electron laser (FEL) is a new generation of laser whose development motivates further research in basic and applied physics. Unlike a conventional laser that uses a gas or solid state gain medium, the FEL gain medium is a relativistic electron beam produced by a particle accelerator. This thesis will explore electron beam dynamics in an FEL, including the beam envelope equation, which will help us understand the evolution of electron betatron motion in the undulator. Dipole magnets, quadrupoles, and solenoids play important roles in transporting and focusing in an FEL beamline. The dipole magnets redirect the electron beam to a beam dump or recirculate the electrons for energy recovery. The quadrupoles and solenoids collimate and focus the electron beam. Simulations and theory are used to model and study a simple FEL beamline.

THIS PAGE INTENTIONALLY LEFT BLANK

TABLE OF CONTENTS

THIS PAGE INTENTIONALLY LEFT BLANK

LIST OF FIGURES

THIS PAGE INTENTIONALLY LEFT BLANK

LIST OF TABLES

THIS PAGE INTENTIONALLY LEFT BLANK

ACKNOWLEDGMENTS

I would like to thank my advisors Professor Blau and Professor Colson. Without your guidance and support, I would never have completed this thesis. Thank you for taking the time to explain the many FEL concepts and review my thesis. I am also grateful to Professor Cohn for your helpful advice and assistance with my writing and simulations.

THIS PAGE INTENTIONALLY LEFT BLANK

I. INTRODUCTION

Compared to conventional lasers, the free electron laser (FEL) is a new generation of laser developed in the mid-1970s by John Madey. Its development not only motivates further research in basic and applied physics (such as accelerator physics), but also broadens the horizon of laser applications in science, medicine, industry, military, etc.

For a traditional laser, the gain medium, pumping mechanism and resonant cavity are the key components. Once the electrons of the gain medium interact with the pumping mechanism, they will be elevated from the ground state to a higher energy (excited) state. The electrons in the excited state then will fall back to the ground state, emitting photons in a process called “spontaneous emission.” Stimulated emission occurs when the excited electrons emit in the presence of photons. Net light amplification can occur when there are more electrons in the excited state than the lower energy state, a condition called “population inversion.” A resonant cavity has mirrors at both ends whose function is to reflect and outcouple the light. One of the mirrors is highly reflective, and the other is partially transparent. The photons generated by spontaneous, or stimulated emission, travel back and forth between the mirrors, which creates more chances to interact with other excited state electrons yielding more and more photons in the cavity. A laser beam is produced as a portion of this amplified light escapes from the partially transparent mirror [1].

In an FEL, a highly-relativistic free electron beam generated by and accelerated from an electron gun and a radio frequency accelerator, respectively, passes through an array of alternating magnets called an undulator. The magnetic fields in the undulator cause the electrons to wiggle and emit photons (spontaneous emission). The function of the optical resonator in an FEL is the same as in a traditional laser, which is to store the photons, provide feedback for stimulated emission, and outcouple the laser beam. The reflected photons interact with the wiggling electrons to produce more light via stimulated emission. The wavelength of FEL radiation depends on the period and strength of the magnetic field in the undulator and the energy of the electrons. By varying any, or all of, these parameters, the wavelength of the laser beam is continuously tunable

over a broad spectrum. Tunable wavelength is an attractive attribute for many FEL applications [2].

The concept of utilizing an FEL as a shipboard weapon brought attention from the United States Navy several decades ago. One of the advantages of an FEL weapon is the energy delivery speed. It can destroy or disable surface and air threats at ranges of ~5 kilometers, delivering the energy at the speed of light. The low cost per shot is another advantage of an FEL over conventional weapons. The cost is only a few dollars for a ~5s FEL engagement. Moreover, an FEL provides a naval ship with a deep magazine. A naval surface ship only can carry and store a finite number of missiles in the launcher and magazine. On the contrary, an FEL is limited only by the amount of power that a ship can provide [2].

In Chapter II, we introduce two types of FELs, an oscillator and an amplifier, as well as their key components. Then, we also discuss the FEL theory which contains the electron equations of motion, pendulum equation, and resonance condition. Electron motion is further explored, including betatron motion in the undulator, focusing by solenoids and quadrupole magnets, bending by dipole magnets, and the beam envelope equation.

Chapter III demonstrates the results of simulations for electron motion passing through dipole magnets, solenoids, quadrupole magnets, and an undulator. In addition, a simulation of the beam envelope shows the evolution of an electron beam through a simple beamline.

Chapter IV summarizes the results found in the present study and suggests future work.

II. FREE ELECTRON LASER OVERVIEW

A. CONFIGURATIONS AND COMPONENTS OF FELs

The oscillator and amplifier are two configurations of an FEL; both types contain an injector, a linear accelerator, an undulator, and a beam dump. Similar to a traditional laser design, an oscillator configuration has an optical resonator consisting of mirrors at both ends in which photons can bounce back and forth to produce more photons (Figure 1). In contrast to an oscillator, an amplifier configuration has no optical resonator. Instead, a seed laser is amplified in a single pass through a longer undulator to generate the laser beam. The following discussion describes the major components of an FEL.

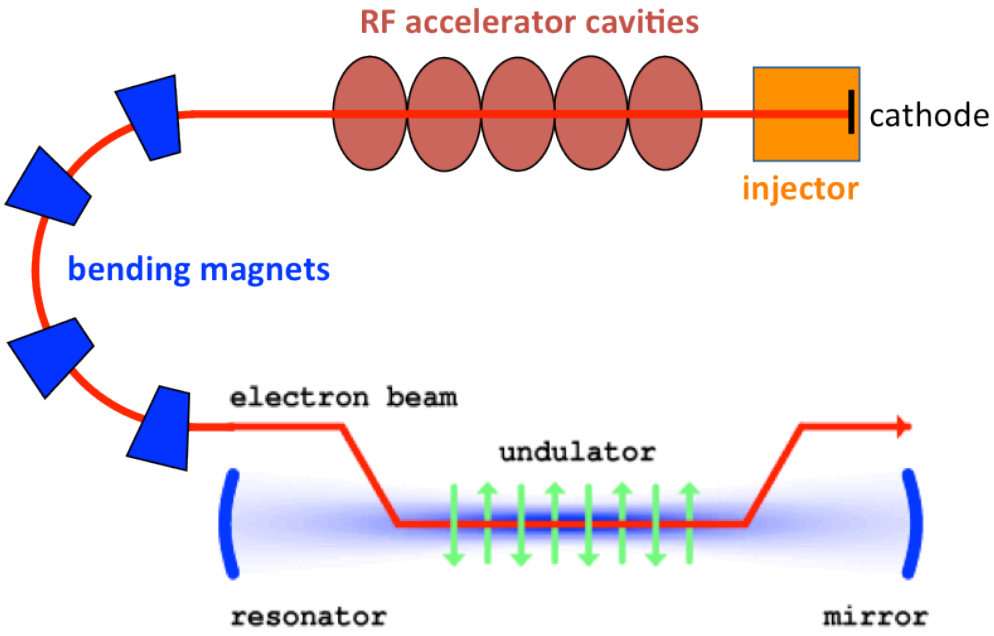

Figure 1. FEL oscillator configuration. The red line indicates the electrons' path starting from the injector to the resonator via the accelerator. Blue wedges are bending magnets used to redirect the electron beam. Alternating magnets in the undulator (green arrows) cause the electrons to wiggle and emit photons, which are stored in the resonator between the mirrors (blue). In the FEL amplifier configuration (not shown in the figure), a seed laser is amplified over a single pass through a longer undulator without the use of a resonator. From [3].

1. Injector

The source of the free electrons in an FEL is an injector (also called an electron gun). An injector consists of a cathode and an anode with a high voltage across them. By either the thermionic or photoelectric effect, electrons can overcome the work function of the material and escape from the cathode into vacuum. An accelerating cavity in the injector may increase the electrons' energy up to ~5 million electron volts (MeV).

2. Accelerator

The well-developed radio frequency linear accelerator (RF linac) is commonly used in FELs. The RF linac consists of a series of cavities in which alternating electric fields are stored at radio frequencies (typically ~300 MHz to ~1 GHz). The low energy electrons (~5 MeV) from the injector passing through the alternating electric fields in the cavities will be repeatedly accelerated to high energies (~100 MeV). The increase of temperature in copper cavities due to the wall currents is an important issue. To reduce wall losses, superconducting cavities made of niobium are immersed in liquid helium at 2–4 K. Figure 2 shows a niobium accelerator cavity.

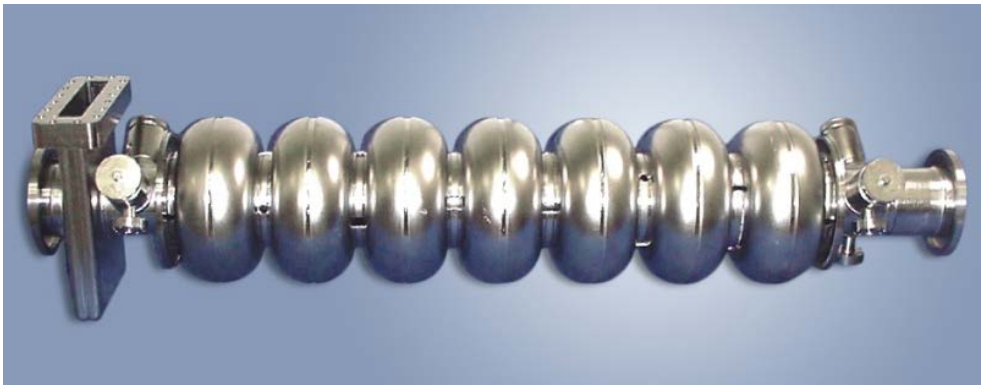

Figure 2. A niobium accelerator cavity. The function of the accelerator cavity is to increase electrons' energy from low (~5 MeV) to high (~100 MeV) through the alternating electric fields. From [4].

3. Undulator

After leaving the accelerator and entering an undulator, highly-relativistic free electrons undergo two types of wiggling motion due to the transverse periodic magnetic

field of the alternating magnets. One type of motion is the fast wiggling motion in each period and the other is the slow betatron motion over many periods. The fast wiggling motion causes electrons to emit photons via spontaneous emission and facilitates coupling between the electron beam and laser light. There are several types of undulators, such as electromagnetic or permanent magnet undulators with helical or linear polarizations. Permanent magnet undulators are now widely used because of their rigid composition and strong magnetic fields. Figure 3 shows a sketch of linearly polarized undulator.

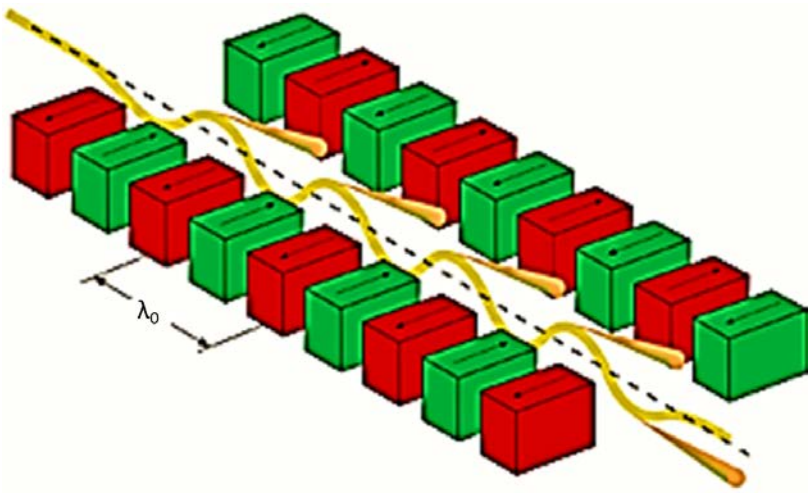

Figure 3. Undulator. The alternating dipole magnet sets (red and green blocks) in an undulator create a periodic magnetic field. The yellow zigzagged line is the electron beam trajectory and the orange cones indicate emitted light. λ_0 is one undulator period. After [5].

4. Resonator

An FEL oscillator has an optical resonator consisting of two mirrors enclosing the undulator in order to store and amplify photons. One of the mirrors is highly reflective and the other is partially transmitting. The amplified, coherent, and collimated light generated by spontaneous and stimulated emission outcouples from the partially transmitting mirror for further use.

B. FEL THEORY

1. Electron Equations of Motion

To understand FEL physics, the transverse and longitudinal motion of electrons in an undulator is an essential topic. To begin the derivation of the electron equations of motion, we first introduce the relativistic Lorentz force equations in cgs units that are given by [2]

$$\frac{d(\gamma\vec{\beta})}{dt} = -\frac{e}{mc}\left(\vec{E} + \vec{\beta}\times\vec{B}\right), \tag{2.1}$$

$$\dot{\gamma} = -\frac{e}{mc}\vec{\beta}\bullet\vec{E}, \tag{2.2}$$

where $\gamma = 1/\sqrt{1-\beta^2}$ is the Lorentz factor, $\beta = \mathrm{v}/c$ is the electron relativistic velocity, m is the electron mass, c is the speed of light, E is the electric field, and B is the magnetic field. Equation (2.2) shows how the electric field can do work on the electrons, increasing or decreasing their energy (γmc^2).

Next, we need to determine the magnetic field in the undulator. As mentioned previously, an undulator has either linear or helical polarizations whose magnetic fields are respectively defined as

$$\vec{B}_l = B_0\left[\sin(k_0 z)\cosh(k_0 y)\hat{y} + \cos(k_0 z)\sinh(k_0 y)\hat{z}\right], \tag{2.3}$$

$$\vec{B}_h = B_0\left[\cos(k_0 z)\hat{x} + \sin(k_0 z)\hat{y}\right], \tag{2.4}$$

where subscripts *l* and *h* stand for linear and helical, B_0 is the magnetic field strength, $k_0 = 2\pi/\lambda_0$ is the undulator wave number, and λ_0 is the undulator period. Electrons complete one wiggle period as they pass through one undulator period λ_0. Figure 4 shows the fields for a linear undulator where the alternating magnets face in the *y* direction and electrons oscillate in the *x* direction as they propagate in the *z* direction. Since the resulting equations of motion for a helical magnetic field in Equation (2.3) are simpler than for a linear one in Equation (2.4), we will assume a helical undulator for the following derivation.

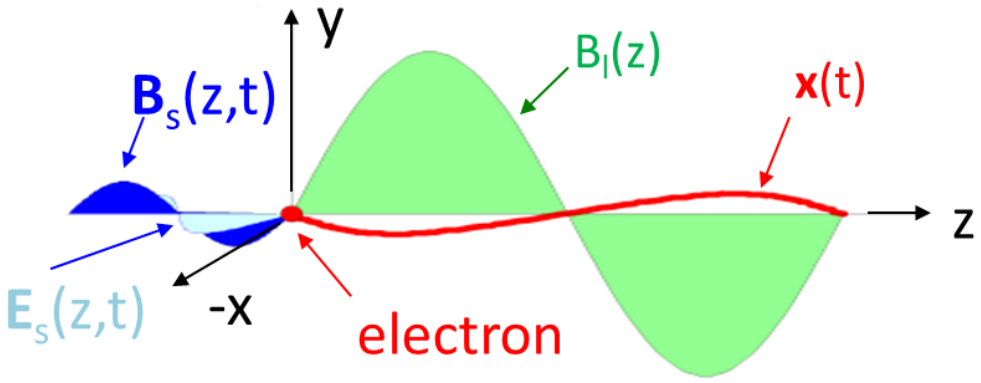

Figure 4. Electric and magnetic fields for a linear undulator. An electron (red dot) starts wiggling motion from the entrance of the undulator, the origin of the coordinate system, travels along the *z* axis, and produces photons. B_s and E_s are the corresponding electric and magnetic fields. B_l is the magnetic field in the undulator. From [3].

The fast-wiggling electrons emit light with electric and magnetic fields given by

$$\vec{E}_s = E\left(\cos\psi\,\hat{x} - \sin\psi\,\hat{y}\right), \tag{2.5}$$

$$\vec{B}_s = E\left(\sin\psi\,\hat{x} + \cos\psi\,\hat{y}\right), \tag{2.6}$$

where E is the electric field strength, $\psi = kz - \omega t + \phi$, $k = 2\pi/\lambda$ is the optical wave number, λ is the optical wavelength, $\omega = kc$ is the optical frequency, and ϕ is the optical phase. Combining Equations (2.4), (2.5), and (2.6), the relativistic Lorentz force equation in Equation (2.1) becomes

$$\frac{d(\gamma\vec{\beta})}{dt} = -\frac{e}{mc}\left[\vec{E}_s + \vec{\beta}\times(\vec{B}_h + \vec{B}_s)\right]$$

$$= -\frac{e}{mc}\left\{E\left(\cos\psi\,\hat{x} - \sin\psi\,\hat{y}\right) + \vec{\beta}\times\left[B_0\left(\cos(k_0 z)\hat{x} + \sin(k_0 z)\hat{y}\right) + E\left(\sin\psi\,\hat{x} + \cos\psi\,\hat{y}\right)\right]\right\},$$

and after expansion we obtain the electron's transverse and longitudinal equations of motion:

$$\frac{d}{dt}(\gamma\beta_x) = -\frac{e}{mc}\left[E\cos\psi(1-\beta_z) - \beta_z B\sin(k_0 z)\right], \tag{2.7}$$

$$\frac{d}{dt}(\gamma\beta_y) = -\frac{e}{mc}\left[-E\sin\psi(1-\beta_z) - \beta_z B\cos(k_0 z)\right], \tag{2.8}$$

$$\frac{d}{dt}(\gamma\beta_z) = -\frac{e}{mc}\left\{E(\beta_x\cos\psi - \beta_y\sin\psi) + B\left[\beta_x\sin(k_0 z) - \beta_y\cos(k_0 z)\right]\right\}. \tag{2.9}$$

Because the relativistic electrons travel at approximately the speed of light, Equations (2.7) and (2.8) can be solved by assuming that there is no light in the undulator ($\dot{\gamma} = 0$), setting $\beta_z \approx 1,$ and integrating with respect to time which yields

$$\beta_x \approx -\frac{K}{\gamma}\cos(k_0 z), \tag{2.10}$$

$$\beta_y \approx -\frac{K}{\gamma}\sin(k_0 z), \tag{2.11}$$

$$\beta_x^2 + \beta_y{}^2 = \frac{K^2}{\gamma^2}, \tag{2.12}$$

where we define the dimensionless undulator parameter $K \equiv eB_{rms}\lambda_0 / 2\pi mc^2$ and B_{rms} is the root-mean-square (rms) magnetic field of the undulator. The value of B_{rms} in the helical undulator is equal to B_0 while the counterpart in the linear undulator is $B_0 / \sqrt{2}.$ In addition, we ignored an integration constant in Equations (2.7) and (2.8) by assuming that electrons are injected into the undulator to propagate along a perfect helical path. Using $z \approx ct$ and integrating again, we obtain the transverse position as a function of time from Equations (2.10) and (2.11):

$$\begin{aligned} x(t) &\approx -\frac{K}{k_0\gamma}\sin(k_0 ct) \qquad y(t) \approx -\frac{K}{k_0\gamma}\cos(k_0 ct) \\ &\approx -\frac{K\lambda_0}{2\pi\gamma}\sin(\omega_0 t) \qquad\qquad \approx -\frac{K\lambda_0}{2\pi\gamma}\cos(\omega_0 t) \end{aligned} \tag{2.13}$$

where $\omega_0 = k_0 c$ is the undulator angular frequency. Note that both relativistic electrons in Equations (2.13) and the electric field of the light in Equation (2.5) have transverse components. Therefore, some electrons move in the same direction as the electric field and some electrons move in the opposite direction to the electric field. Since electrons carry negative charges, the speeds of electrons moving in the same direction as the electric field will decrease. On the other hand, the speeds of electrons moving in the opposite direction to the electric field will increase. Increasing speeds of electrons means they acquire energy and decreasing speeds of electrons means they lose energy to the electric field. Thus, some electrons gain energy and some lose energy due to the random distribution of electrons. This phenomenon of energy exchange causes electrons to bunch.

To understand energy exchange between the electrons and the electric field, we can insert Equations (2.5), (2.10) and (2.11) into Equation (2.2) and get

$$\begin{aligned}\frac{d\gamma}{dt} = \dot{\gamma} &= -\frac{e}{mc}\left[-\frac{K}{\gamma}\cos(k_0 z)\hat{x} - \frac{K}{\gamma}\sin(k_0 z)\hat{y}\right]\bullet\left[E\left(\cos\psi\,\hat{x} - \sin\psi\,\hat{y}\right)\right] \\ &= \frac{eKE}{\gamma mc}\cos(k_0 z + \psi) \\ &= \frac{eKE}{\gamma mc}\cos(k_0 z + kz - \omega t + \phi) \\ &= \frac{eKE}{\gamma mc}\cos(\zeta + \phi), \end{aligned} \tag{2.14}$$

where $\zeta \equiv (k_0 + k)z - \omega t$ is the electron phase which represents the electron microscopic position in an optical wavelength. If $\dot{\gamma}$ is greater than zero, electrons increase energy and if $\dot{\gamma}$ is less than zero electrons lose energy.

2. Resonance

Based on the previous discussion, the fast-wiggling electrons in the undulator moving in the same direction as the electric field lose energy and those moving in the opposite direction to the electric field gain energy. Due to the speed difference between the electron and photon, the photon will advance ahead of the electron a distance of one wavelength λ over one undulator period (Figure 5). This will result in optimum energy exchange between the electrons and the light, a condition known as resonance.

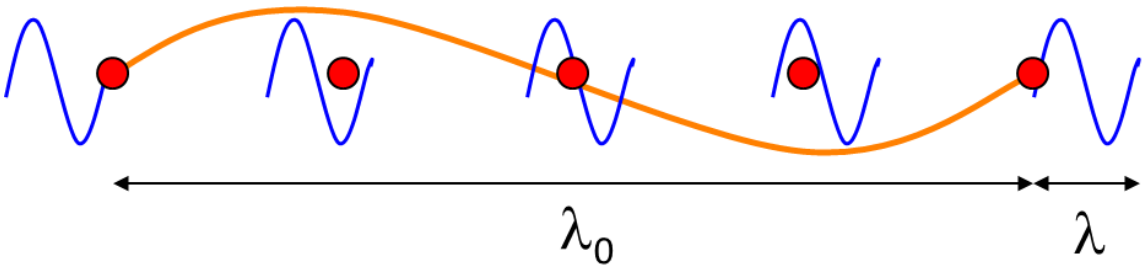

Figure 5. The electron-photon race. As the electron (red dot) completes one oscillation (the orange path) in one undulator period λ_0, a photon (blue) passes over the electron, winning the "race" over the electron by a distance of one wavelength of light λ. From [3].

The resonance condition is a significant concept of an FEL and can be expressed mathematically as

$$\left(\frac{\lambda_0}{\mathrm{v}}\right)c = \lambda_0 + \lambda. \tag{2.15}$$

Using $\beta_z = \mathrm{v}/c$ and Equation (2.12), we can write the FEL resonance condition in a more practical form as

$$\begin{aligned}\lambda &= \frac{\lambda_0(1-\beta_z)}{\beta_z} \\ &\approx \frac{\lambda_0(1+K^2)}{2\gamma^2},\end{aligned} \tag{2.16}$$

where $\beta_z = \sqrt{1-(1+K^2)/\gamma^2} \approx 1-(1+K^2)/2\gamma^2$ by binomial expansion. Equation (2.16) illustrates that the wavelength λ of an FEL is tunable over a broad spectrum by adjusting the undulator period λ_0, the undulator parameter K, or the electron energy γmc^2.

3. Pendulum Equation and Phase Space Evolution

To simplify the electron equations of motion, we first define the dimensionless time τ and an operator $\overset{\circ}{(..)}$ to denote the derivative with respect to τ :

$$\tau \equiv ct/L, \tag{2.17}$$

$$\overset{\circ}{(..)} \equiv \frac{d(..)}{d\tau} = \frac{L}{c}\frac{d}{dt}, \tag{2.18}$$

where $L = N\lambda_0$ is the undulator length, which means that τ goes from 0 to 1 over the length of the undulator. The derivative of electron phase ζ with respect to dimensionless time τ yields electron phase velocity ν,

$$\begin{aligned}\nu &\equiv \frac{d\zeta}{d\tau} = \overset{\circ}{\zeta} \\ &= \frac{L}{c}\frac{d}{dt}\left[(k_0+k)z - \omega t\right] \\ &= L\left[(k+k_0)\beta_z - k\right].\end{aligned} \tag{2.19}$$

Next, we take the derivative of electron phase velocity ν with respect to dimensionless time τ again and get

$$\begin{aligned}
\overset{\circ}{\nu} &= \frac{L}{c}\frac{d}{dt}\left\{L\left[(k+k_0)\beta_z - k\right]\right\} \\
&= \frac{L^2(k+k_0)}{c}\frac{d\beta_z}{dt} \\
&\approx \frac{L^2 k}{c}\frac{d}{dt}\left[\frac{1+K^2}{2\gamma^2}\right] \\
&\approx \frac{L(N\lambda_0)}{c}\left[\frac{4\pi\gamma^2}{\lambda_0(1+K^2)}\right]\left[\frac{(1+K^2)\dot{\gamma}}{\gamma^3}\right] \\
&\approx \frac{L}{c}\frac{4\pi N}{\gamma}\dot{\gamma}, \qquad (2.20)
\end{aligned}$$

where we assume $k \gg k_0$ near resonance and apply $k = 4\pi\gamma^2 / \lambda_0(1+K^2)$ from Equation (2.16). The final step is to substitute $\dot{\gamma}$ in Equation (2.14) into Equation (2.20) and we can get the pendulum equation

$$\overset{\circ}{\nu} = \overset{\circ\circ}{\zeta} = |a|\cos(\zeta + \phi), \qquad (2.21)$$

where $|a| = 4\pi NeKLE / \gamma^2 mc^2$ is the dimensionless optical field. The magnitude of the dimensionless optical field $|a|$ influences electron bunching. Weak fields occur when $|a|$ is less than π, which causes weak electron bunching. On the other hand, $|a|$ comparable to or greater than π implies strong fields and strong electron bunching. The pendulum equation describes the microscopic motion of electrons in terms of electron phase ζ and electron phase velocity ν.

Electron phase space evolution in the undulator (Figure 6) can explain resonance. Twenty sample electrons shown in red dots of Figure 6 are uniformly distributed in phase ζ as they travel through the undulator. The phase velocity ν and the electron phase ζ represent electron energy and electron microscopic position in an optical wavelength respectively. At resonance, electrons' initial phase velocities are zero at the entrance of the undulator. After entering the undulator, electrons begin fast-wiggling motion and energy exchange with optical field. At the end of the undulator, half of the electrons'

phase velocities increase, which means electrons gain energy from the optical field. The other half of the electrons' phase velocities decrease, which means electrons lose energy to the optical field. Although electron bunching occurs at resonance, total energy exchange between the electrons and the optical field in the end is zero. In other words, there is no optical gain.

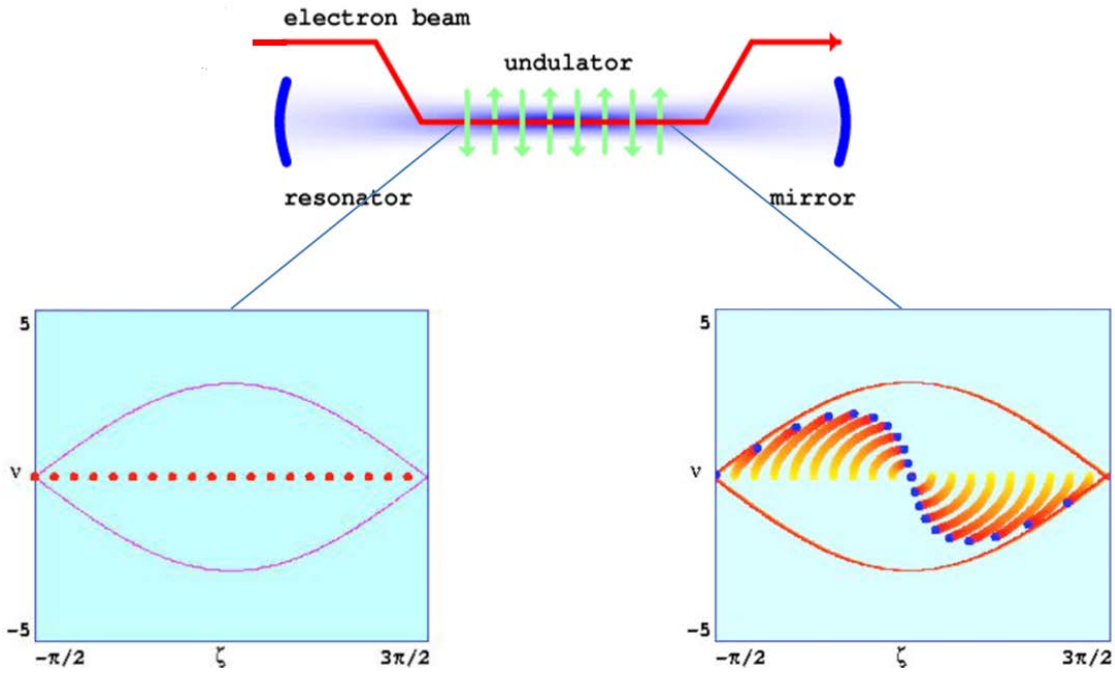

Figure 6. Electron phase space evolution at resonance (20 sample electrons). Red arrowed line is the electron beam passing through the undulator. Bottom left window shows initial phase velocity of each electron (red dot) is zero. Bottom right window shows the final phase velocity and position of each electron (blue dot). There is no net energy exchange between the electrons and the optical field at resonance. From [3].

For achieving net gain, electrons transferring energy to the optical field should outnumber those acquiring energy from the optical field. One method to achieve this occasion is that electrons enter the undulator with higher energy or above resonance. Figure 7 is an example of 200 sample electrons (blue dots) uniformly distributed in phase ζ as they pass through the undulator. Different from Figure 6, electrons have higher initial phase velocities since they carry higher energy at the entrance of the undulator. Then, individual electrons will evolve in accordance with the pendulum equation in

Equation (2.21). The final electron positions in Figure 7 indicate that the total number of electrons losing energy to the optical field is more than the number of electrons gaining energy, so net gain occurs.

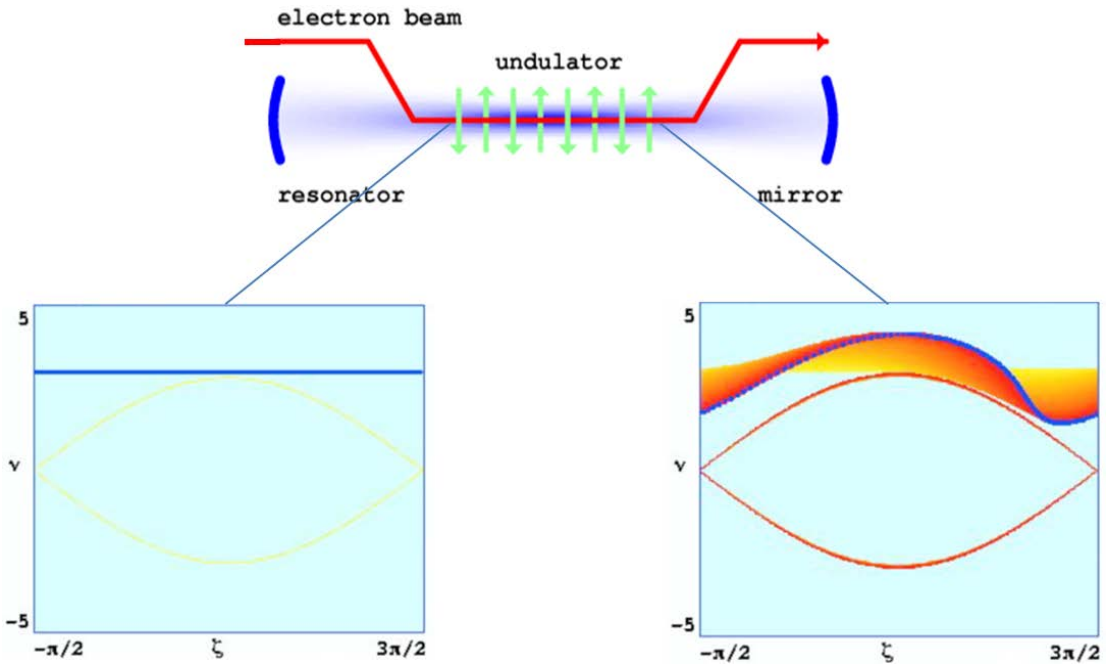

Figure 7. Electron phase space evolution above resonance (200 sample electrons). Red arrowed line is the electron beam passing through the undulator. Bottom left window shows each electron (blue dot) has higher initial phase velocity. Bottom right window shows the final phase velocity and position of each electron (blue dot). Above resonance, most of the electrons transfer energy to the optical field so net gain occurs. From [3].

4. Betatron Motion

In this section, we will explore another electron motion in the undulator called betatron motion caused by the transverse variation in the magnetic field of the undulator. We begin the derivation by assuming that the electron is moving in a linear undulator whose magnetic field is defined in Equation (2.3). Inserting Equation (2.3) into the relativistic Lorentz equation, Equation (2.1), and neglecting forces due to light in the undulator ($\dot{\gamma} = 0$) yields

$$\dot{\vec{\beta}} = \frac{-e}{\gamma mc}\Big[(\beta_y B_z - \beta_z B_y)\hat{x} - \beta_x B_z \hat{y} + \beta_x B_y \hat{z}\Big]. \tag{2.22}$$

From Equation (2.3), the x-component of Equation (2.22) can be written as

$$\begin{aligned}\dot{\beta}_x &= \frac{-eB_0}{\gamma mc^2}\big[\dot{y}\cos(k_0 z)\sinh(k_0 y) - \dot{z}\sin(k_0 z)\cosh(k_0 y)\big] \\ &= \frac{-eB_0}{\gamma mc^2}\frac{1}{k_0}\frac{d}{dt}\big[\cos(k_0 z)\cosh(k_0 y)\big]. \end{aligned}\tag{2.23}$$

Next, we integrate Equation (2.23) with respect to time and obtain

$$\beta_x = \frac{-eB_0}{k_0\gamma mc^2}\cos(k_0 z)\cosh(k_0 y) + C, \tag{2.24}$$

where C is a constant. We assume that electrons are injected into the undulator to propagate along a perfect sinusoidal path, which leads to $C = 0$. Also, it is assumed that $k_0 y \ll 1$ so that the electrons remain near the undulator axis and $\cosh(k_0 y) \approx 1$. With the above assumptions and the previous definition of the dimensionless linear undulator parameter $K = eB_0 / (\sqrt{2}k_0 mc^2)$, Equation (2.24) is then simplified to

$$\beta_x \approx \frac{-eB_0}{k_0\gamma mc^2}\cos(k_0 z) \tag{2.25}$$

$$\approx \frac{-\sqrt{2}K}{\gamma}\cos(k_0 z)$$

$$\approx \frac{-\sqrt{2}K}{\gamma}\cos(k_0\beta_0 ct), \tag{2.26}$$

where $z \approx \beta_0 ct \approx ct$. We can use Equation (2.26) and $k_0 = 2\pi / \lambda_0$ to find x:

$$\beta_x = \frac{\mathrm{v}_x}{c} \approx -\frac{\sqrt{2}K}{\gamma}\cos(k_0 ct)$$

$$\rightarrow \mathrm{v}_x \approx -\frac{\sqrt{2}Kc}{\gamma}\cos(k_0 ct)$$

$$\rightarrow \quad x \approx -\frac{\sqrt{2}Kc}{k_0\gamma}\sin(k_0 ct) + x_0$$

$$\approx -\frac{K\lambda_0}{\sqrt{2}\pi\gamma}\sin(k_0 ct) + x_0,$$

where x_0 is the initial displacement. We assumed that electrons inject into the undulator perfectly, so $x_0 = 0$. Therefore,

$$x \approx -\frac{K\lambda_0}{\sqrt{2}\pi\gamma}\sin(k_0 ct). \tag{2.27}$$

Equation (2.27) describes the fast wiggling motion of the electrons, with period $\lambda_0 \approx$ few centimeter and amplitude ≈ 0.1 millimeter for a typical FEL.

Next, we use the previous method to obtain the y-component of Equation (2.22)

$$\dot{\beta}_y = \frac{\sqrt{2}K}{\gamma} k_0 \dot{x}\cos(k_0 z)\sinh(k_0 y).$$

Using $\dot{x} = \beta_x c,\ \ \beta_x = -\sqrt{2}K\cos(k_0 z)/\gamma,$ and a trigonometric identity, we can write

$$\begin{aligned}\dot{\beta}_y &= \frac{-2cK^2}{\gamma^2} k_0 \cos^2(k_0 z)\sinh(k_0 y)\cosh(k_0 y) \\ &= \frac{-cK^2 k_0}{\gamma^2}\cos^2(k_0 z)\sinh(2k_0 y).\end{aligned}$$

The average value of $\cos^2(k_0 z)$ over many periods is $1/2$. By assuming that $k_0 y \ll 1$ as before, we can write the average value of $\dot{\beta}_y$ as

$$\begin{aligned}\left\langle \dot{\beta}_y \right\rangle &= \frac{-cK^2 k_0}{2\gamma^2}\sinh(2k_0 y) \\ &\approx \frac{-cK^2 k_0^2}{\gamma^2} y \\ \rightarrow c\left\langle \dot{\beta}_y \right\rangle = \left\langle \ddot{y} \right\rangle &\approx -\frac{c^2 K^2 k_0^2}{\gamma^2} y.\end{aligned} \tag{2.28}$$

Equation (2.28) is the form of simple harmonic motion. We rewrite Equation (2.28) using dimensionless time τ :

$$\overset{\circ\circ}{y} = -\left(\frac{Kk_0 L}{\gamma}\right)^2 y = -\omega_\beta^2 y \tag{2.29}$$

where ω_β is the dimensionless betatron frequency

$$\omega_\beta = \frac{Kk_0 L}{\gamma} = \frac{2\pi NK}{\gamma} \tag{2.30}$$

Equation (2.29) describes the electrons' slow betatron motion in the undulator. In a typical FEL, $N \approx 100$, $K \approx 1$, and $\gamma \approx 100$, so $\omega_\beta \approx 2\pi$, which corresponds to one oscillation over the length of the undulator ($\Delta\tau = 1$). Additionally, the general solution of Equation (2.29) is

$$y(\tau) = y_0 \cos(\omega_\beta \tau) + \frac{L\theta_{y_0}}{\omega_\beta} \sin(\omega_\beta \tau), \tag{2.31}$$

where y_0 is the electron initial transverse position at $\tau = 0$, $\theta_{y_0} = \overset{\circ}{y}(0)/L$ is the initial tilted angle of the electron velocity from the z axis at $\tau = 0$, and $\overset{\circ}{y}(0)$ is the initial electron velocity at $\tau = 0$. Equation (2.31) will be applied to simulation program of electron betatron motion in Chapter III.

5. Envelope Equation in an Undulator

In the previous section, we showed that an individual electron undergoes betatron motion in an undulator. Another approach to study the evolution of an electron beam in a betatron field is to consider the beam envelope. We start the derivation of the beam envelope equation [6] from electron betatron motion defined in Equation (2.29). Multiplying by y and averaging over the distribution, Equation (2.29) becomes

$$\left\langle y \overset{\circ\circ}{y} \right\rangle = -\omega_\beta^2 \left\langle y^2 \right\rangle \tag{2.32}$$

where $\langle \alpha \rangle = \frac{1}{n}\sum_{i=1}^{n} \alpha_i$. Defining the dimensionless standard deviation of the electron positions as σ_y and the electron angular spreads as $\sigma_{\theta y}$, we can write σ_y^2 and $\sigma_{\theta y}^2$ as

$$\sigma_y^2 = \frac{1}{n}\sum_{i=1}^{n} y_i^2 = \left\langle y^2 \right\rangle, \tag{2.33}$$

$$\sigma_{\theta y}^2 = \frac{1}{n}\sum_{i=1}^{n} \left(\overset{\circ}{y}_i \right)^2 = \left\langle \overset{\circ}{y}^2 \right\rangle. \tag{2.34}$$

Using Equations (2.32), (2.33), and (2.34), we find the term $\frac{d}{d\tau}\left\langle y \overset{\circ}{y} \right\rangle$ can be expressed as

$$\begin{aligned}
\frac{d}{d\tau}\left\langle y\,\dot{y}\right\rangle &= \frac{1}{n}\frac{d}{d\tau}\sum_{i=1}^{n} y_i\,\dot{y}_i \\
&= \frac{1}{n}\sum_{i=1}^{n}\left(\dot{y}_i^{\,2} + y_i\,\ddot{y}_i\right) \\
&= \frac{1}{n}\sum_{i=1}^{n}\left(\dot{y}_i\right)^2 + \frac{1}{n}\sum_{i=1}^{n}\left(y_i\,\ddot{y}_i\right) \\
&= \left\langle \dot{y}^{\,2}\right\rangle + \left\langle y\,\ddot{y}\right\rangle \\
&= \left\langle \dot{y}^{\,2}\right\rangle - \omega_\beta^2\left\langle y^2\right\rangle \\
&= \sigma_{\theta y}^2 - \omega_\beta^2\sigma_y^2. \qquad (2.35)
\end{aligned}$$

Furthermore, from the chain rule and Equation (2.33), $\frac{d}{d\tau}\left\langle y\,\dot{y}\right\rangle$ can be written as

$$\begin{aligned}
\frac{d}{d\tau}\left\langle y\,\dot{y}\right\rangle &= \frac{1}{n}\frac{d}{d\tau}\sum_{i=1}^{n} y_i\,\dot{y}_i \\
&= \frac{1}{2}\frac{d^2}{d\tau^2}\left(\frac{1}{n}\sum_{i=1}^{n} y_i^2\right) \\
&= \frac{1}{2}\frac{d^2}{d\tau^2}\left\langle y^2\right\rangle \\
&= \frac{1}{2}\frac{d^2}{d\tau^2}\left(\sigma_y^2\right) \\
&= \frac{d}{d\tau}\left(\sigma_y\,\dot{\sigma}_y\right) \\
&= \sigma_y\,\ddot{\sigma}_y + \left(\dot{\sigma}_y\right)^2. \qquad (2.36)
\end{aligned}$$

Combining Equations (2.35) and (2.36) results in

$$\sigma_{\theta y}^2 - \omega_\beta^2\sigma_y^2 = \sigma_y\,\ddot{\sigma}_y + \left(\dot{\sigma}_y\right)^2,$$

$$\sigma_y\,\ddot{\sigma}_y + \omega_\beta^2\sigma_y^2 - \frac{\sigma_y^2\sigma_{\theta y}^2 - \left(\sigma_y\,\dot{\sigma}_y\right)^2}{\sigma_y^2} = 0,$$

$$\ddot{\sigma}_y + \omega_\beta^2\sigma_y - \frac{\varepsilon_y^2}{\sigma_y^3} = 0, \qquad (2.37)$$

where we define the dimensionless rms beam emittance $\varepsilon_y^2 = \sigma_y^2 \sigma_{\theta y}^2 - (\sigma_y \overset{\circ}{\sigma}_y)^2$. Next, we can rewrite Equation (2.37) in term of 4-rms beam width and arrive at

$$\overset{\circ\circ}{Y} + \omega_\beta^2 Y - \frac{\varepsilon_Y^2}{Y^3} = 0 \tag{2.38}$$

where $Y = 4\sigma_y$ and $\varepsilon_Y = 16\varepsilon_y$. Equation (2.38) is the dimensionless beam envelope equation in an undulator and will be applied to the simulation program with electron betatron motion in Chapter III.

C. BEAMLINE COMPONENTS

1. Quadrupole Magnets

The function of a quadrupole magnet (Figure 8) is to focus electrons as well as to keep the electron beam aligned before entering the undulator. Typically, pairs or triplets of quadrupole magnets are set in the beamline of the FEL in order to focus the electrons.

Figure 8. A quadrupole triplet. Focusing characteristic makes quadrupole magnet a significant component in an FEL beamline. The four brown coils mounted on yellow shell create quadrupole magnetic field to focus electrons. A long FEL beamline consists of many sets of quadrupole doublet or triplet of quadrupole for the sake of maintaining transporting electron within the beam pipe. From [7].

Figures 9 and 10 depict two configurations of quadrupole magnets, and their magnetic fields (red arrows). The propagation direction of electrons in Figures 9 and 10 is out of the page. When passing through the quadrupole magnet in Figure 9, electrons will be defocused in the *x* direction and focused in the *y* direction simultaneously (blue arrows) due to the magnetic force. In contrast, electrons will be defocused in the *y* direction and focused in the *x* direction simultaneously if we switch the positions of north and south poles of the quadrupole magnet (Figure 10). Next, we will discuss the equations of motion for electrons in a quadrupole magnet based on the configuration in Figure 9.

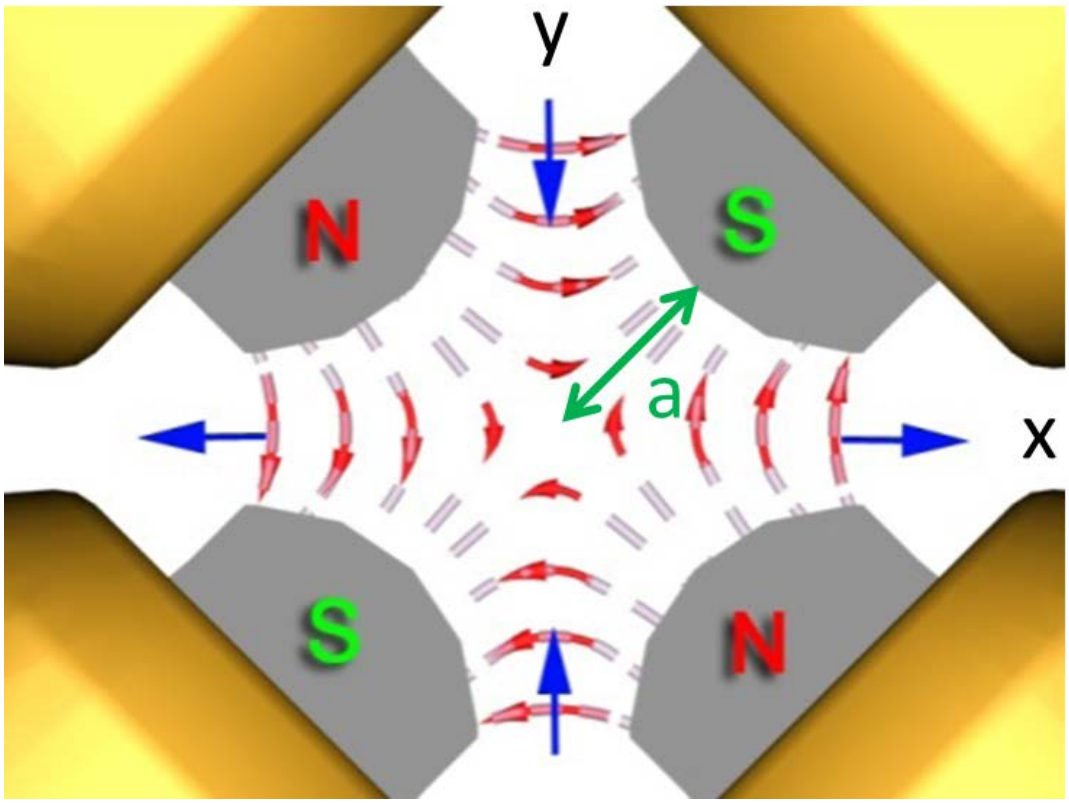

Figure 9. Quadrupole magnet. Red arrows are the magnetic field lines and blue arrows are the direction of force. In this configuration, an electron moving out of the page through the quadrupole is defocused in the horizontal direction and focused in the vertical direction. After [8].

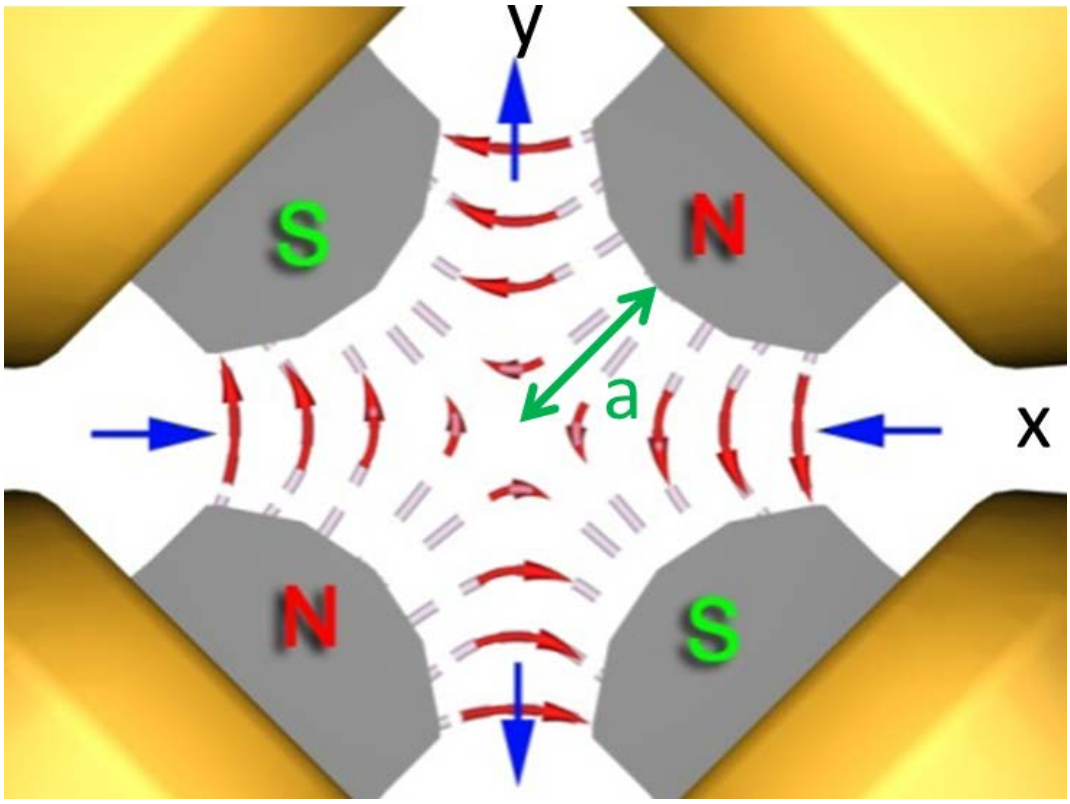

Figure 10. Quadrupole magnet. Red arrows are the magnetic field lines and blue arrows are the direction of force. In this configuration, an electron moving out of the page through the quadrupole is focused in the horizontal direction and defocused in the vertical direction. After [8].

The electric field in a quadrupole magnet is zero, and magnetic fields do no work ($\dot{\gamma} = 0$), so the relativistic Lorentz force equation, Equation (2.1), can be written as

$$\dot{\vec{\beta}} = \frac{-e}{\gamma mc}\left[\left(\beta_y B_z - \beta_z B_y\right)\hat{x} + \left(\beta_x B_z - \beta_z B_x\right)\hat{y} + \left(\beta_x B_y - \beta_y B_x\right)\hat{z}\right]. \tag{2.39}$$

We simplify Equation (2.39) by assuming that electrons travel through an ideal quadrupole magnet ($B_z \approx 0$) at nearly the speed of the light, so $\beta_z \approx 1$, and $\beta_x \approx \beta_y \ll \beta_z$. Equation (2.39) becomes

$$\dot{\vec{\beta}} \approx \frac{-e}{\gamma mc}\left[-B_y\hat{x} + B_x\hat{y}\right]. \tag{2.40}$$

A magnetic quadrupole field is given by

$$B_x = B_q \frac{y}{a}, \qquad B_y = B_q \frac{x}{a}, \tag{2.41}$$

where a is the distance from the axis to the pole surface and B_q is the maximum field strength when $x = a$ or $y = a$ (Figure 9). From Equation (2.41), we can obtain the x and y components of the relativistic Lorentz force equation:

$$\begin{aligned}
\dot{\beta}_x &\approx \frac{e}{\gamma mc} B_y \qquad & \dot{\beta}_y &\approx -\frac{e}{\gamma mc} B_x \\
\rightarrow \dot{\mathrm{v}}_x &\approx \frac{e}{\gamma m} B_y & \dot{\mathrm{v}}_y &\approx -\frac{e}{\gamma m} B_x \\
\rightarrow \quad \ddot{x} &\approx \frac{eB_q}{a\gamma m} x & \ddot{y} &\approx -\frac{eB_q}{a\gamma m} y \\
\rightarrow \quad \ddot{x} &\approx \omega_q^2 x & \ddot{y} &\approx -\omega_q^2 y,
\end{aligned} \tag{2.42}$$

where $\omega_q^2 \equiv eB_q / a\gamma m$. Equation (2.42) describes the motion of electrons in the quadrupole magnet of Figure 9. It also indicates that electrons are defocused in the x direction and focused in the y direction, as expected. Based on these characteristics, the quadrupole magnet can be considered as an optical thin lens, so we will continue by deriving the equivalent lens formula.

First, we rewrite Equations (2.42) in terms of dimensionless time τ:

$$\begin{aligned}
\overset{\circ\circ}{x} &\approx \frac{eL^2 B_q}{a\gamma mc^2} x \qquad & \overset{\circ\circ}{y} &\approx -\frac{eL^2 B_q}{a\gamma mc^2} y \\
&\approx \kappa x & &\approx -\kappa y
\end{aligned} \tag{2.43}$$

where $\kappa \equiv eL^2 B_q / a\gamma mc^2$. When an electron passes through the quadrupole magnet, its transverse velocity v_x is changed according to

$$\begin{aligned}
\mathrm{v}_{x_2} &\approx \mathrm{v}_{x_1} + \int_{\tau_1}^{\tau_2} \overset{\circ}{\mathrm{v}} d\tau \\
&\approx \mathrm{v}_{x_1} + \int_{\tau_1}^{\tau_2} \overset{\circ\circ}{x} d\tau \\
&\approx \mathrm{v}_{x_1} + \int_{\tau_1}^{\tau_2} \kappa x d\tau,
\end{aligned}$$

where v_{x_1} and v_{x_2} stand for the electron's velocities and τ_1 and τ_2 are the dimensionless times at entrance and at exit of the quadrupole magnetic field. Compared to its longitudinal velocity, the electron's transverse velocity v_x is relatively small. The length of the quadrupole field is small, so we can assume that *x* is constant as the electron travels through the quadrupole magnet. Thus,

$$\begin{aligned} v_{x_2} &\approx v_{x_1} + \kappa(\tau_2 - \tau_1)x \\ &\approx v_{x_1} + (\kappa\Delta\tau)x. \end{aligned} \tag{2.44}$$

where $\Delta\tau = \tau_2 - \tau_1 = L_q / L$ and L_q is the length of the quadrupole. To derive an equivalent lens formula for a quadrupole magnet, we define $1/f \equiv \kappa\Delta\tau$ and rewrite Equation (2.44) as

$$v_{x_2} \approx v_{x_1} + \frac{x}{f}. \tag{2.45}$$

where f (>0 in this case) represents the focal length of the quadrupole magnet. Likewise,

$$v_{y_2} \approx v_{y_1} - \frac{y}{f}. \tag{2.46}$$

Equation (2.45) and (2.46) show that a quadrupole magnet arranged as in Figure 9 will focus the electron in the *y* direction and defocus in the *x* direction. Next, we will discuss a combination of two quadrupole magnets (a doublet) shown in Figure 11 and its equivalent lens formula.

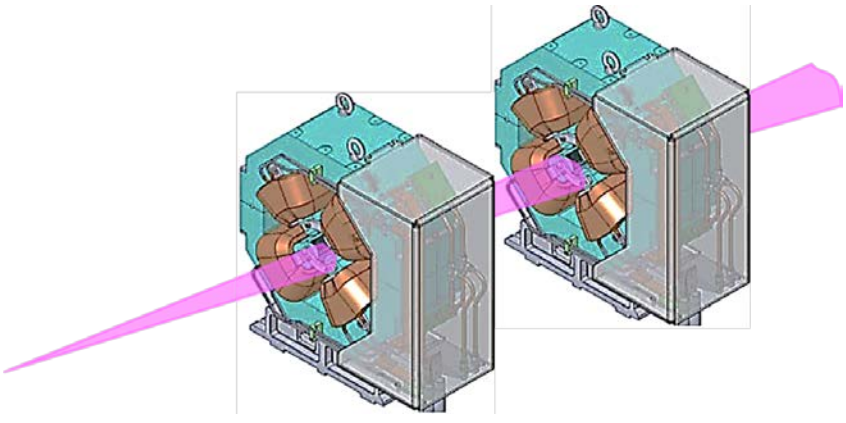

Figure 11. Quadrupole doublet. After [8].

We assume f_1 and f_2 are the focal lengths of two quadrupole magnets separated by a short distance *d*. The equivalent lens formula then becomes

$$\frac{1}{F}=\frac{1}{f_1}+\frac{1}{f_2}-\frac{d}{f_1 f_2}, \tag{2.47}$$

where *F* is the equivalent focal length of the doublet. If these two quadrupole magnets have identical field strength and are arranged like Figure 11 ($f_1 = f$ and $f_2 = -f$) , Equation (2.47) will become

$$\frac{1}{F}=\frac{d}{f^2}. \tag{2.48}$$

A quadrupole triplet consists of three quadrupole magnets, where the focal length of the second magnet is f and focal lengths of the first and third magnet is $-2f$, respectively.

2. Solenoid Lens

A solenoid is another device commonly used to focus the electron beam, due to its axisymmetric magnetic field. Assuming electrons propagate along the z direction and enter a solenoid magnetic field along the *z*-axis as shown in Figure 12, the radial component of the field will deflect electrons azimuthally toward the z axis. Thus, like a quadrupole, a solenoid can be treated as a focusing lens.

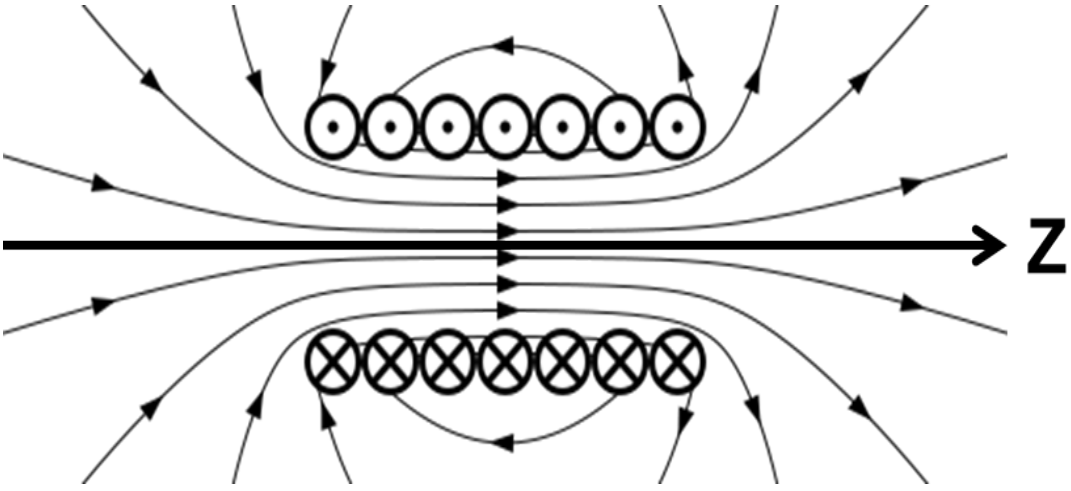

Figure 12. Schematic picture of a solenoid magnetic field. After [9].

The relativistic Lorentz force equation in cylindrical coordinates (r, θ, z) is

$$\frac{d}{dt}\left(\gamma m\dot{\vec{r}}\right) = -e\dot{\vec{r}} \times \vec{B},$$

$$\left(\ddot{r} - r\dot{\theta}^2\right)\hat{\mathbf{r}} + \left(2\dot{r}\dot{\theta} + r\ddot{\theta}\right)\hat{\boldsymbol{\theta}} + \ddot{z}\hat{\mathbf{z}} = -\frac{e}{\gamma m}\left[\left(r\dot{\theta}B_z - \dot{z}B_\theta\right)\hat{\mathbf{r}} + \left(\dot{z}B_r - \dot{r}B_z\right)\hat{\boldsymbol{\theta}} + \left(\dot{r}B_\theta - r\dot{\theta}B_r\right)\hat{\mathbf{z}}\right],$$

$$\left(\ddot{r} - r\dot{\theta}^2\right)\hat{\mathbf{r}} + \left(2\dot{r}\dot{\theta} + r\ddot{\theta}\right)\hat{\boldsymbol{\theta}} + \ddot{z}\hat{\mathbf{z}} = -\frac{e}{\gamma m}\left[r\dot{\theta}B_z\hat{\mathbf{r}} + \left(\dot{z}B_r - \dot{r}B_z\right)\hat{\boldsymbol{\theta}} - r\dot{\theta}B_r\hat{\mathbf{z}}\right], \qquad (2.49)$$

where component $B_\theta = 0$ since the magnetic field of a solenoid is axially symmetric. From Equation (2.49) the radial, azimuthal, and axial motions of an electron are

$$\ddot{r} - r\dot{\theta}^2 = -\frac{e}{\gamma m}\left(r\dot{\theta}B_z\right), \qquad (2.50)$$

$$2\dot{r}\dot{\theta} + r\ddot{\theta} = -\frac{e}{\gamma m}\left(\dot{z}B_r - \dot{r}B_z\right), \qquad (2.51)$$

$$\ddot{z} = \frac{e}{\gamma m}\left(r\dot{\theta}B_r\right). \qquad (2.52)$$

Equation (2.50) describes how the solenoid focuses the electron. However, its expression shows the electron radial motion with respect to time. What we actually need is the electron radial motion related to z, so we have to rewrite Equation (2.50) in terms of r and $r' = dr/dz$.

The longitudinal field B_z and radial field B_r in the paraxial approximation are given by [6]

$$B_z \approx B_s(z), \qquad (2.53)$$

$$B_r \approx -\frac{1}{2}rB_s'(z), \qquad (2.54)$$

where $B_s(z)$ is the longitudinal magnetic field for the solenoid and the prime denotes a derivative with respect to z. Applying $\dot{B}_s = B_s'\dot{z}$ and Equations (2.53) and (2.54), Equation (2.51) can be rewritten as

$$\frac{1}{r}\left(2r\dot{r}\dot{\theta} + r^2\ddot{\theta}\right) = -\frac{e}{\gamma m}\left(\dot{z}B_r - \dot{r}B_z\right)$$

$$= \frac{e}{2\gamma m}\left[r\dot{z}B_s'(z) + 2\dot{r}B_s(z)\right]$$

$$= \frac{e}{2\gamma mr}\left[r^2 \dot{B}_s(z) + 2r\dot{r}B_s(z)\right]$$

$$\rightarrow \frac{d}{dt}\left(r^2\dot{\theta}\right) = \frac{e}{2\gamma m}\frac{d}{dt}\left[r^2 B_s(z)\right]. \tag{2.55}$$

By integrating Equation (2.55) with respect to time, we get

$$\dot{\theta} = \frac{e}{2\gamma m}B_s(z) \tag{2.56}$$

where we set the integration constant to zero by assuming the electron trajectory is very close to the axis. Substituting Equations (2.52), (2.53), (2.54) and (2.56) into Equation (2.50) results in

$$\ddot{r} = -\frac{e^2}{4\gamma^2 m^2} r B_s^2(z)$$

$$\rightarrow r''\dot{z}^2 + r'\ddot{z} = -\frac{e^2}{4\gamma^2 m^2} r B_z^2(z)$$

$$\rightarrow r'' + \left(\frac{eB_s(z)}{2\beta\gamma mc}\right)^2 r = 0$$

$$\rightarrow r'' + k_s^2 r = 0 \tag{2.57}$$

where we assume $\ddot{z} = 0$ in the case of a simple magnetic field, and $k_s = eB_s(z)/2\beta\gamma mc$. Equation (2.57) describes the electron motion in the solenoid magnetic field and is known as the paraxial ray equation [6]. Integrating Equation (2.57) with respect to z yields

$$r_2' - r_1' = -\int_{z_1}^{z_2} k_s^2 r dz, \tag{2.58}$$

where r_2' and r_1' indicate the slope of the electron trajectory at longitudinal positions $z = z_2$ and $z = z_1$ respectively. Assuming that the electron trajectory does not cross the z axis, the left side term $r_2' - r_1'$ in Equation (2.58) is negative because k_s^2 and r are positive. Hence, the slope r_1' at position z_1 is greater than the slope r_2' at position z_2, which means that the solenoid will focus the beam. Using the thin lens approximation and assuming $r_1' = 0$ and $r_2' = r'$, Equation (2.58) can be rewritten as

$$
\begin{aligned}
r' &= -\int_{z_1}^{z_2} k_s^2 r dz \\
&= -r_s \left(\frac{e}{2\beta\gamma mc} \right)^2 \int_{z_1}^{z_2} B_s^2(z) dz \\
&= -r \left(\frac{eB_s}{2\beta\gamma mc} \right)^2 L_s
\end{aligned} \tag{2.59}
$$

where we assume the magnetic field $B_s(z)$ is constant and L_s is the length of the solenoid. Then the focal length f_s of the solenoid lens is defined as [6]

$$
\begin{aligned}
\frac{1}{f_s} &= -\frac{r'}{r} \\
&= \left(\frac{eB_s}{2\beta\gamma mc} \right)^2 L_s \\
&= \left(\frac{e\mu_0 n_s I_s}{2\beta\gamma mc} \right)^2 L_s
\end{aligned} \tag{2.60}
$$

where we assume $B_s = \mu_0 n_s I_s$ for an ideal solenoid [10], μ_0 is the permeability of free space, n_s is the number of turns per unit solenoid length, and I_s is the current. As an example, if $\gamma = 3$, $\beta = 0.94$, total current $n_s I_s = 30\text{kA}$ with length $L_s = 6.5\text{cm}$ of the solenoid, Equation (2.60) yields the dimensionless focal length $f_s = 1\text{m}$. Note that the focal length f_s in Equation (2.60) is proportional to the electron energy squared, so the solenoid lens is only suitable for focusing electrons with low energy [11]. For the following simulation, we rewrite Equation (2.60) in terms of dimensionless focal length $\tilde{f}_s$ as

$$
\begin{aligned}
\tilde{f}_s &= \frac{f_s}{L} \\
&= \left(\frac{2\beta\gamma mc}{e\mu_0 n_s I_s} \right)^2 \frac{1}{LL_s},
\end{aligned} \tag{2.61}
$$

where L is the length of the undulator.

3. Dipole Magnet

The purpose of dipole magnets in an FEL beamline is to change the direction of the electron beam. Examples of their use are to bend the electrons around the cavity mirrors of an undulator, to direct the beam into the beam dump, or to recirculate the beam for energy recovery. Consider a dipole magnet (Figure 13) consisting of two bar magnets that produce a homogenous magnetic field pointing in the positive y direction. Assume the electron beam propagates in the positive z direction (perpendicular to the y axis) through the midplane of the two magnets. According to the Lorentz force equation in Equation (2.1) and ignoring fringe effects of the dipole magnet, the magnetic field of the dipole magnet will deflect the electron beam in the positive x direction.

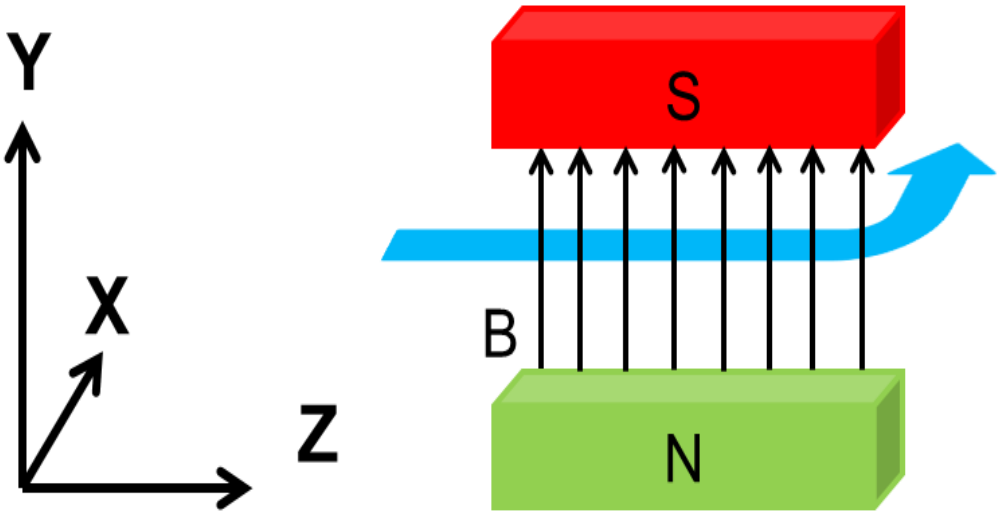

Figure 13. Dipole magnet. A dipole magnet creates a uniform magnetic field pointing in the positive y direction. The electron beam is initially moving in the positive z direction, perpendicular to the magnetic field, and travels through the middle of the field. The electron beam is deflected in the positive x direction due to the Lorentz force.

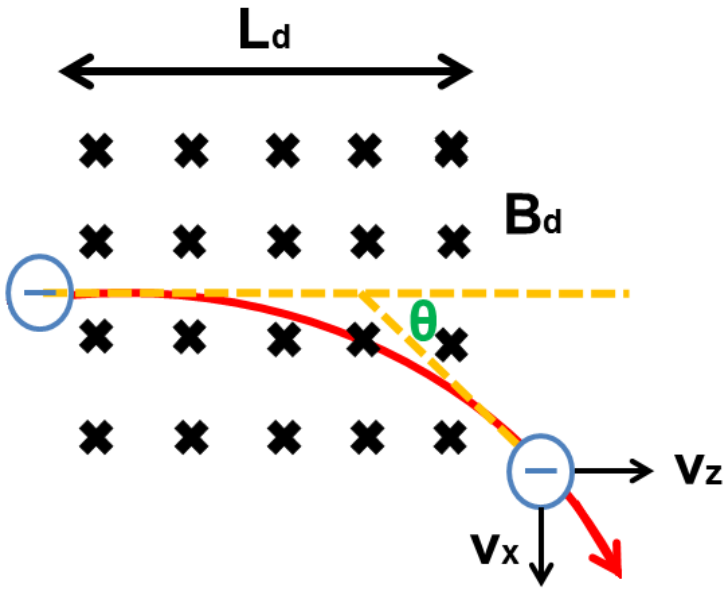

Figure 14. Electron motion in a uniform magnetic field. An electron travels in the positive z direction through a uniform magnetic field (into the page) perpendicular to the electron motion. The red circular line indicates the path of the electron due to the magnetic field. The deflection angle θ of the electron is the ratio of v_x to v_z.

To determine the deflection angle of the electron beam, assume an electron initially traveling along the positive *z*-axis with speed v enters the dipole magnet where the uniform magnetic field is perpendicular to the electron (Figure 14). The relativistic Lorentz force on the electron is

$$\frac{d}{dt}\left(\gamma m \vec{\mathrm{v}}\right) = -e\vec{\mathrm{v}}\times\vec{B}_d$$
$$\rightarrow \frac{d\vec{\mathrm{v}}}{dt} = \frac{d\,\mathrm{v}_x}{dt}\hat{x} + \frac{d\,\mathrm{v}_z}{dt}\hat{z} = \frac{eB_d}{\gamma m}\left(\mathrm{v}_z\,\hat{x} - \mathrm{v}_x\,\hat{z}\right) \qquad (2.62)$$

where subscript *d* denotes the dipole magnet and B_d is the magnetic field strength. By taking the derivative of Equation (2.62) with respect to time t, we get

$$\frac{d^2\vec{\mathrm{v}}}{dt^2} = \frac{eB_d}{\gamma m}\left(\frac{d\,\mathrm{v}_z}{dt}\hat{x} - \frac{d\,\mathrm{v}_x}{dt}\hat{z}\right)$$
$$= -\left(\frac{eB_d}{\gamma m}\right)^2\left(\mathrm{v}_x\,\hat{x} + \mathrm{v}_z\,\hat{z}\right)$$
$$= -\omega_c^2\left(\mathrm{v}_x\,\hat{x} + \mathrm{v}_z\,\hat{z}\right) \qquad (2.63)$$

where $\omega_c = eB_d / \gamma m$ is the cyclotron frequency. Equation (2.63) can be solved analytically with the initial conditions $\mathrm{v}_x(0) = 0$ and $\mathrm{v}_z(0) = \beta c$. The solutions are

$$\mathrm{v}_x = \beta c \sin \omega_c t, \tag{2.64}$$

$$\mathrm{v}_z = \beta c \cos \omega_c t, \tag{2.65}$$

$$x = -\frac{\beta c}{\omega_c} \cos \omega_c t, \tag{2.66}$$

$$z = \frac{\beta c}{\omega_c} \sin \omega_c t. \tag{2.67}$$

The ratio of v_x to v_z in Equations (2.64) and (2.65) determines the deflection angle θ,

$$\tan\theta = \frac{\mathrm{v}_x}{\mathrm{v}_z} = \tan \omega_c t,$$

$$\theta = \omega_c t. \tag{2.68}$$

Next, assuming the electrons pass through the entire magnetic field ($z = L_d$) as shown in Figure 14, and applying Equation (2.66), gives

$$L_d = \frac{\beta c}{\omega_c} \sin \omega_c t. \tag{2.69}$$

Substituting Equation (2.68) into Equation (2.69), and solving for the deflection angle θ, yields

$$\theta = \sin^{-1}\left(\frac{L_d \omega_c}{\beta c}\right)$$

$$= \sin^{-1}\left(\frac{eB_d L_d}{\beta \gamma mc}\right). \tag{2.70}$$

Equations (2.66) and (2.67) show that the electron will follow circular motion in the xz plane. The radius of curvature r_d is

$$r_d = \sqrt{x^2 + z^2}$$

$$= \frac{\beta c}{\omega_c}$$

$$= \left(\frac{\beta \gamma mc}{eB_d}\right). \tag{2.71}$$

Therefore, we can rewrite Equation (2.70) in terms of r_d as

$$\theta = \sin^{-1}\left(\frac{L_d}{r_d}\right). \tag{2.72}$$

Equation (2.72) is valid only if the radius of curvature r_d is greater than the field length L_d, i.e., if the deflection angle $\theta < 90$ degrees. As an example, if $\gamma = 3$, $\beta = 0.94$, and the magnetic field $B_d = 0.085\,\mathrm{T}$ with length $L_d = 0.4\,\mathrm{m}$ of the dipole magnet, Equation (2.72) yields the deflection angle $\theta = 45$ degrees.

III. SIMULATIONS

A. BETATRON MOTION WITH BEAM ENVELOPE

1. Betatron Motion Simulation

Professors J. Blau and W. B. Colson wrote the *betaxy.c* program using the C programming language to simulate betatron motion of electrons in the undulator. Equations (2.31) describing electrons trajectories are solved numerically and all parameters used in the *betaxy.c* program are dimensionless. The program produces plots of dimensionless $x(\tau)$ and $y(\tau)$ for sample electrons. The input parameters σ_x and σ_y are the dimensionless standard deviation of the electron transverse position spreads in x and y. The parameters $\sigma_{\theta x}$ and $\sigma_{\theta y}$ are the dimensionless standard deviation of the electron angular spreads in x and y. The parameters σ_x, σ_y, $\sigma_{\theta x}$, and $\sigma_{\theta y}$ are all defined at the beam waist, at location $\tau = \tau_\beta$, from which the simulation starts calculating and plotting electron trajectories. The parameters $\omega_{\beta x}$ and $\omega_{\beta y}$ are the dimensionless betatron frequencies in the undulator defined in Equation (2.30).

Figure 15 displays a simulation example of fifty electrons undergoing betatron motion as τ goes from 0 to 1 assuming that the undulator magnets are shaped for equal focusing. Each red line indicates one sample electron trajectory. The values of dimensionless betatron frequencies $\omega_{\beta x} = \omega_{\beta y} = \pi$, which means the electrons perform one half of a betatron oscillation over the length of the undulator. The input values of angular spread $\sigma_{\theta x} = \sigma_{\theta y} = 6$, and the input of transverse spread $\sigma_x = \sigma_y = 0.2$. In a typical FEL oscillator, the light is focused in the center of the undulator. Therefore, the parameter $\tau_\beta = 0.5$ at which the electron trajectories are focused.

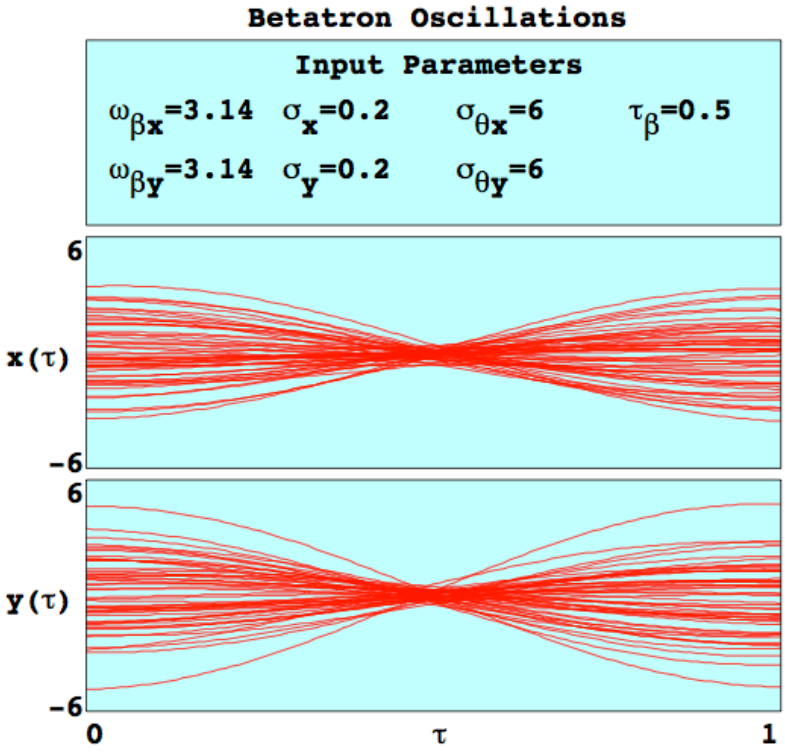

Figure 15. A simulation example of electron betatron motion.

2. Betatron Motion with Beam Envelope Simulation

To simulate electron betatron motion, including the envelope equation defined in Equation (2.38), I developed the new *betaxy-env.c* program by modifying the *betaxy.c* program. Figure 16 is a simulation output of electron betatron motion and beam envelope as τ goes from 0 to 1 along the length of the undulator. The input values of betatron frequencies $\omega_{\beta x}$, $\omega_{\beta y}$, the angular spread $\sigma_{\theta x}$, $\sigma_{\theta y}$, the transverse spread σ_x, σ_y, and τ_β are the same as Figure 15. The program follows the trajectories of 500 sample electrons from $\tau = 0 \rightarrow 1$ according to Equation (2.31) and then calculates the beam envelope using the Euler-Cromer method. The red lines are the electrons' betatron trajectories and the black bold lines are the beam envelope. The graphic output shows that electron trajectories are surrounded by the beam envelope, as expected.

To verify the *betaxy-env.c* program, I revised it by adding the 4-rms of the electron beam and used the same input values in Figure 16. The program plots the beam

envelope and the 4-rms of the electron beam trajectories as thin lines to make them distinguishable. Figure 17 is the simulation result in which the black lines represent the beam envelope equation and the blue lines are the 4-rms of the electron beam trajectories sampled. The graph shows that both curves in *x* and *y* almost match. Moreover, I conducted another simulation with 5000 sample electrons, and the output (not shown) indicates that the beam envelope and the 4-rms of the electron beam overlap more exactly.

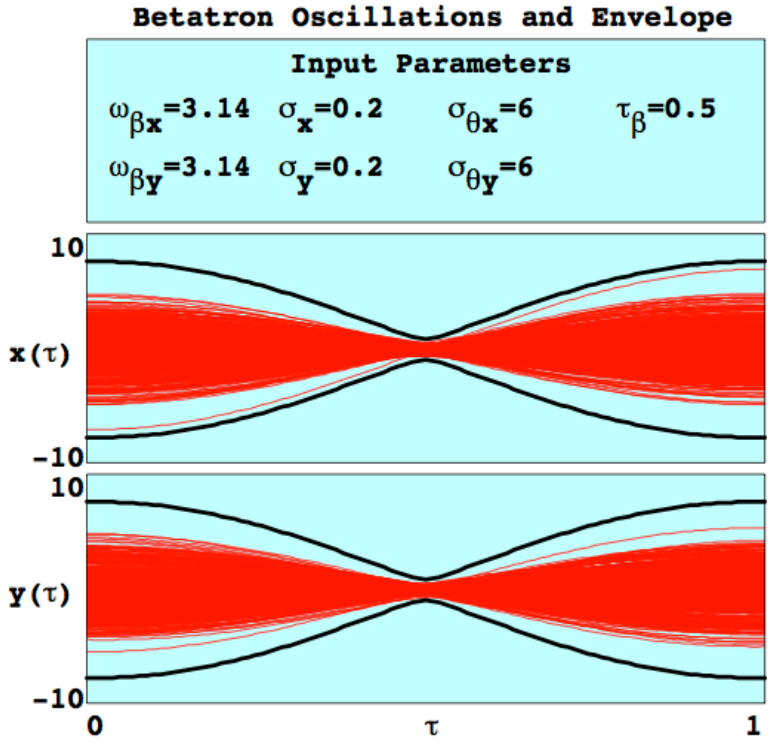

Figure 16. A simulation output of electron betatron motion and the beam envelope.

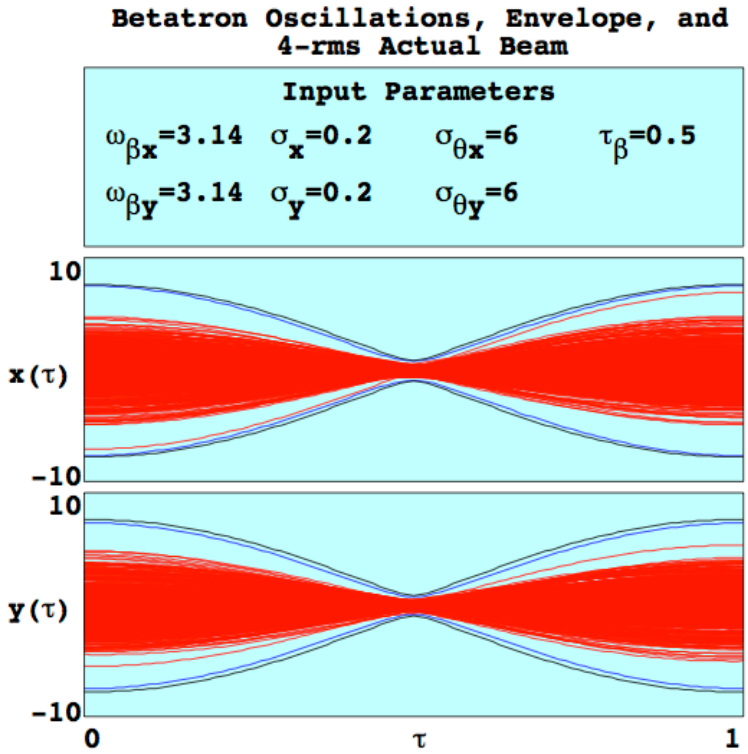

Figure 17. Simulation example of electron betatron motion, the beam envelope, and 4-rms of the actual electron beam.

B. QUADRUPOLE AND UNDULATOR WITH BEAM ENVELOPE

The *quadbetaxy.c* program was developed by a previous student [12] to simulate electron motion through pairs or triplets of quadrupole magnets and then into the undulator. The input parameters σ_x, σ_y, $\sigma_{\theta x}$, $\sigma_{\theta y}$, $\omega_{\beta x}$, $\omega_{\beta y}$, and τ_β have been introduced in the previous section. From the study in Chapter II, a quadrupole magnet can be treated as a thin lens. Therefore, the additional parameters f_1, f_2, and f_3 are focal lengths for quadrupoles and τ_{f1}, τ_{f2}, and τ_{f3} are the corresponding positions of each quadrupole. The *quadbetaxy.c* program simulates the electron trajectories along the undulator ($\tau = 0 \rightarrow 1$) and then completes each trajectory by plotting backward from $\tau = 0 \rightarrow -3$ through a quadrupole doublet or triplet.

Figure 18 depicts a graphic output of 100 sample electrons through a quadrupole triplet and an undulator. Red lines indicate electron trajectories, the green line is the entrance of the undulator ($\tau = 0$), and the three purple lines are the positions of three

quadrupoles. The dimensionless betatron frequencies $\omega_{\beta x} = \omega_{\beta y} = \pi$ so each electron completes half of a betatron oscillation in the undulator ($\tau = 0 \rightarrow 1$). The angular spreads $\sigma_{\theta x} = \sigma_{\theta y} = 3$ and transverse spreads $\sigma_x = \sigma_y = 0.2$. The electron trajectories are focused in the middle of the undulator ($\tau_\beta = 0.5$). The first and third quadrupoles are arranged as in Figure 9, where electrons are defocused in the *x* direction and focused in the *y* direction. They are located at $\tau_{f1} = -1.6$, and $\tau_{f3} = -1.4$ with equal focal length $f_1 = f_3 = 0.6$. The second quadrupole is arranged as in Figure 10, where electrons are focused in the *x* direction and defocused in the *y* direction. Its position is at $\tau_{f2} = -1.5$ with focal length $f_2 = -0.3$. Note that the focal length of the second magnet is half of the first and third magnets and also has an opposite sign. In this combination, the three quadrupoles form a triplet.

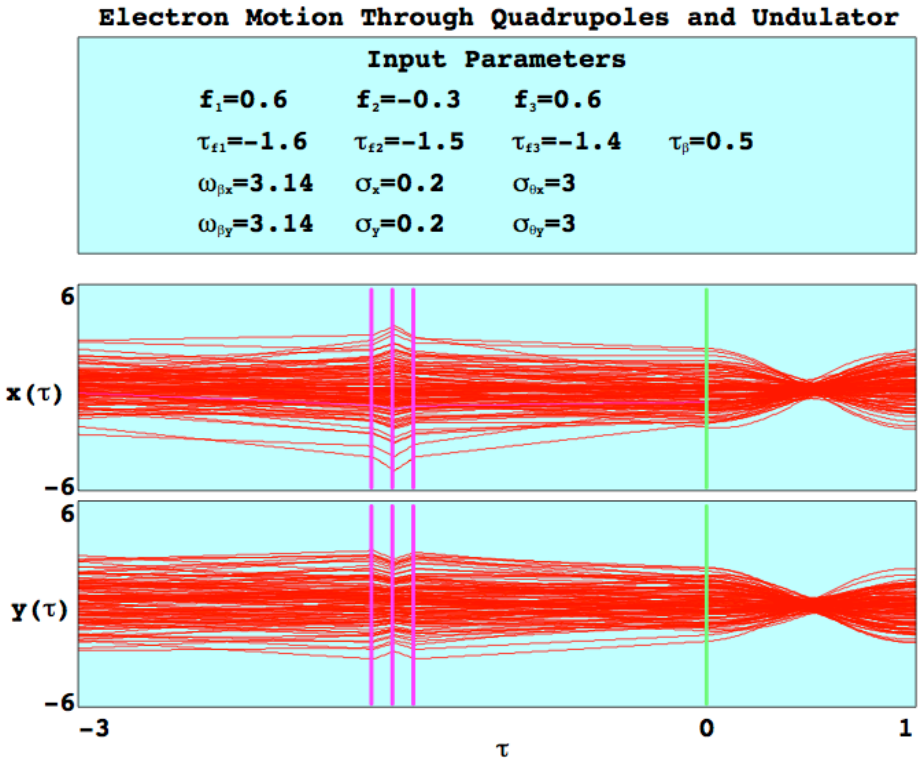

Figure 18. A simulation result of electron betatron motion through three quadrupole magnets and an undulator.

The *quadbetaxy-env.c* program was developed by modifying the *quadbetaxy.c* program simulates electron trajectories and the beam envelope through a quadrupole doublet or triplet and an undulator. Figure 19 shows a simulation result of the *quadbetaxy-env.c* program with 500 sample electrons. The input values of betatron frequencies $\omega_{\beta x}$, $\omega_{\beta y}$, the angular spread $\sigma_{\theta x}$, $\sigma_{\theta y}$, the transverse spread σ_x, σ_y, the focal lengths of quadrupoles f_1, f_2, f_3, the positions of quadrupoles τ_{f1}, τ_{f2}, τ_{f3}, and τ_β, are all the same as in Figure 18. The Euler-Cromer method is applied to calculate the beam envelope in the undulator and through the three quadrupoles. The beam envelope (black bold lines) are defocused in the *x* direction and focused in the *y* direction while passing through the first and third quadrupole, and are focused in the *x* direction and defocused in the *y* direction while passing through the second quadrupole.

To compare with the 4-rms of the electron beam trajectories sampled, I revised the *quadbetaxy-env.c* program and ran it with same input values as in Figure 19. The simulation output is shown in Figure 20. The black lines are the beam envelope and the blue lines are the 4-rms of the electron beam. Both curves in *x* and *y* are nearly identical. Again, another simulation with 5000 sample electrons was made, and the output (not shown) shows that the beam envelope and the 4-rms of the electron beam overlap more exactly.

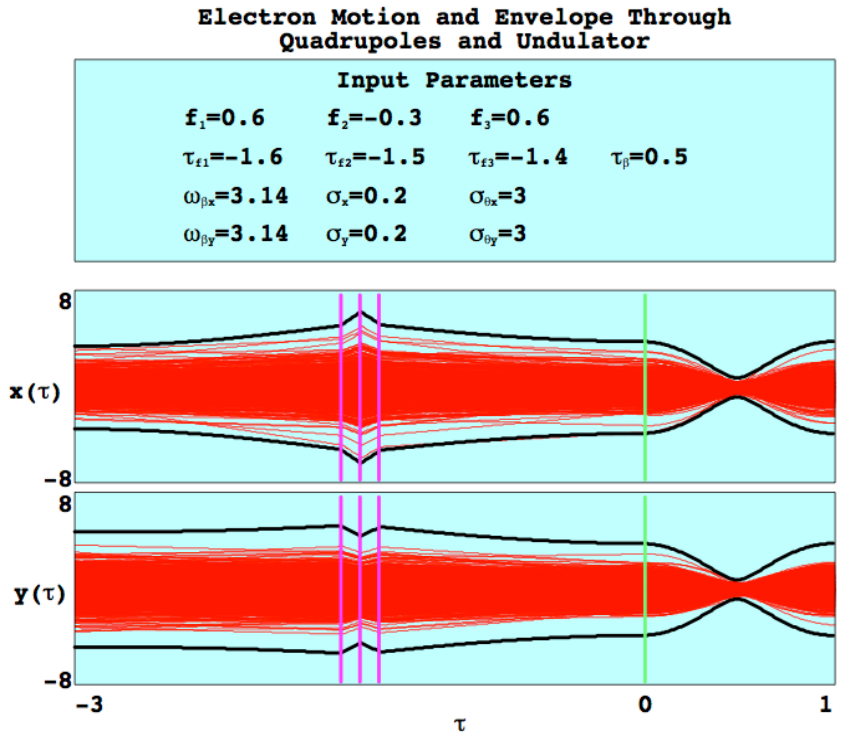

Figure 19. A graphic output of 500 sample electrons traveling through a quadrupole triplet, and an undulator, including the beam envelope.

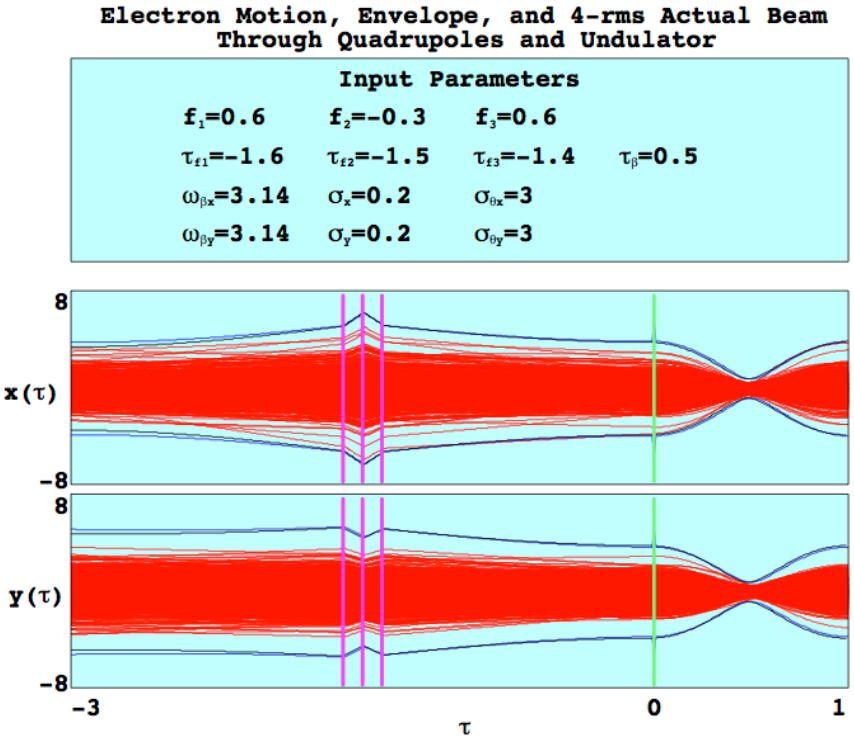

Figure 20. Simulation output of the beam envelope and the 4-rms electron beam.

C. QUADRUPOLE, UNDULATOR, AND DIPOLE MAGNET WITH BEAM ENVELOPE

After leaving the undulator, the electron beam can be steered by dipole magnets to a beam dump or recirculated back to the accelerator for energy recovery. In order to simulate the electron path from an undulator through a dipole magnet as in Figure 13, I further modified the *quadbetaxy-env.c* program and developed the *quadbetadipole-env.c* program. It contains electron trajectories and the beam envelope through quadrupoles and an undulator from $\tau = -3 \rightarrow 1$ and extends them through a dipole magnet to $\tau = 3$. The input parameters σ_x, σ_y, $\sigma_{\theta x}$, $\sigma_{\theta y}$, $\omega_{\beta x}$, $\omega_{\beta y}$, f_1, f_2, f_3, τ_{f1}, τ_{f2}, τ_{f3}, and τ_β have been discussed in the early sections. Three parameters τ_d, ϕ_x, and ϕ_y are added to model the dipole magnet. The parameter τ_d describes the position of the dipole magnet. The parameters ϕ_x and ϕ_y are the transverse bending angles in x and y, normalized to a characteristic angle $\sqrt{\lambda / L\pi}$.

Two simulation outputs of the *quadbetadipole-env.c* program are provided. Figure 21 shows the electron beam deflecting only in x but not y and Figure 22 shows the opposite case. Both cases show 500 sample electrons propagating through a quadrupole triplet, an undulator, and a dipole magnet. Red lines are electron trajectories, the black bold lines are beam envelopes, the green lines are the start and end of the undulator ($\tau = 0$ and 1), the three purple lines are the positions of three quadrupoles (τ_{f1}, τ_{f2}, and τ_{f3}), and the blue line is the position of the dipole magnet (τ_d). The input values $\omega_{\beta x}$, $\omega_{\beta y}$, f_1, f_2, f_3, and τ_β in Figures 21 and 22 are the same as Figure 18, but the values of angular spreads $\sigma_{\theta x}$, $\sigma_{\theta y}$ and transverse spreads σ_x, σ_y are smaller. Hence, compared to Figure 19, the electron beams in Figures 21 and 22 are narrower in both x and y. The position of the dipole magnet is at $\tau_d = 2$ in both Figures 21 and 22. The normalized bending angles are $\phi_x = 1.5$ and $\phi_y = 0$ in Figure 21 and $\phi_x = 0$ and $\phi_y = 1.5$ in Figure 22.

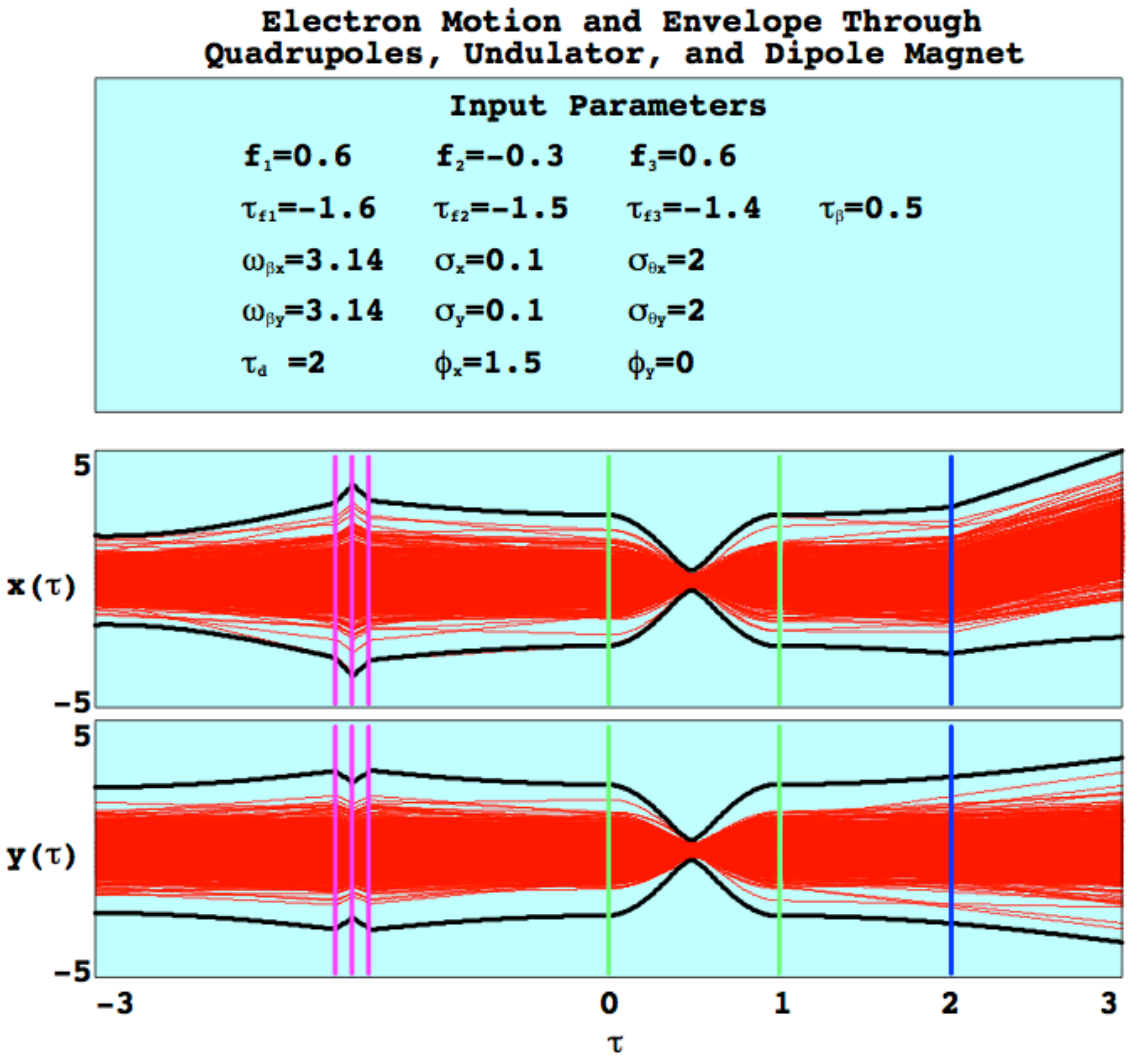

Figure 21. A simulation example of electron betatron motion through a quadrupole triplet, an undulator, and a dipole magnet, including the beam envelope. The result indicates that the electron beam changes direction only in *x*.

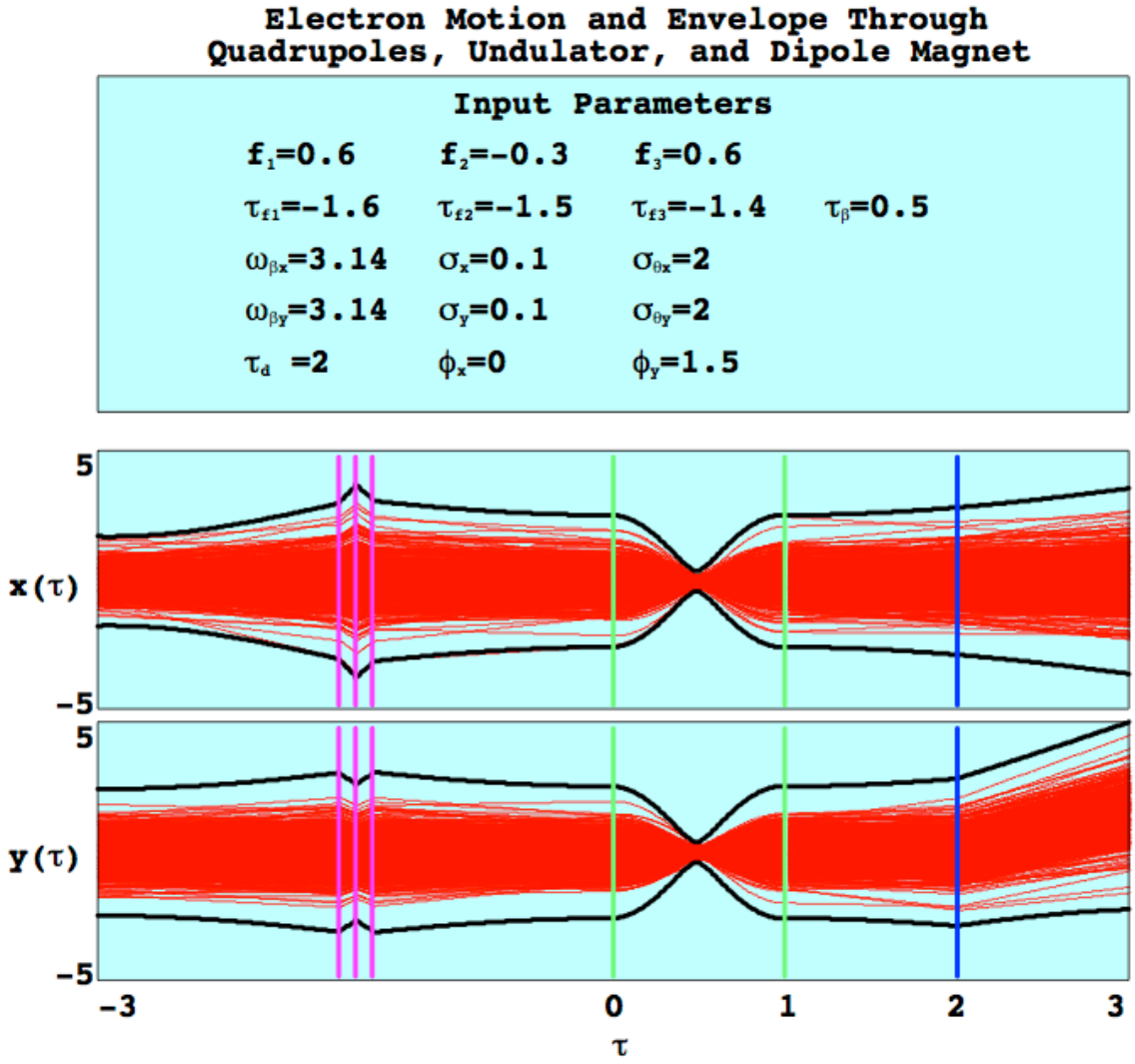

Figure 22. A graphic output of 500 sample electrons trajectories through a quadrupole triplet, an undulator, and a dipole magnet, including the beam envelope. The result shows that the electron beam redirect only in *y*.

D. SOLENOID, UNDULATOR, AND DIPOLE MAGNET WITH BEAM ENVELOPE

Regarding focusing of an electron beam, a quadrupole only has either horizontal or vertical focusing, whereas a solenoid focuses in both directions simultaneously. In some cases, its axial symmetric focusing behavior can be treated as a thin lens. Electron motion in a solenoidal magnetic field and the definition of the focal length for a solenoid were discussed in the last chapter. I rewrote the *quadbetadipole-env.c* program and developed the *solebetadipole-env.c* program by replacing quadrupole lenses with a

solenoid lens to simulate focusing due to a solenoid. The *solebetadipole-env.c* program can simulate electron trajectories and the beam envelope through a solenoid, an undulator, and a dipole magnet. The functions of the input parameters σ_x, σ_y, $\sigma_{\theta x}$, $\sigma_{\theta y}$, $\omega_{\beta x}$, $\omega_{\beta y}$, τ_β, τ_d, ϕ_x, ϕ_y and γ in the *solebetadipole-env.c* program are the same as in the previous simulations. The focusing effect of the solenoid is modeled by two additional parameters f_s and τ_s. The parameter f_s determines the focal length of the solenoid and the parameter τ_s is the corresponding position of the solenoid.

Figure 23 is the simulation result of the *solebetadipole-env.c* program employing 500 sample electrons. The electron trajectories and the beam envelope cover the solenoid region ($\tau = -3 \to 0$), an undulator ($\tau = 0 \to 1$), and a dipole magnet region ($\tau = 1 \to 3$). Electron trajectories are plotted in red, the start and end of the undulator ($\tau = 0$ and 1) are shown by green vertical lines, the position of the solenoid (τ_s) is shown by a yellow vertical line, and the position of the dipole magnet (τ_d) is shown by a blue vertical line. The input values σ_x, σ_y, $\sigma_{\theta x}$, $\sigma_{\theta y}$, $\omega_{\beta x}$, $\omega_{\beta y}$, ϕ_x, ϕ_y, τ_β, τ_d, and γ in Figures 23 are the same as Figure 21. The position of the solenoid is set at $\tau_s = -1.5$ with focal length $f_s = 1.5$. The graphic output indicates that the electron trajectories and the beam envelope converge both in x and y simultaneously after passing the solenoid lens.

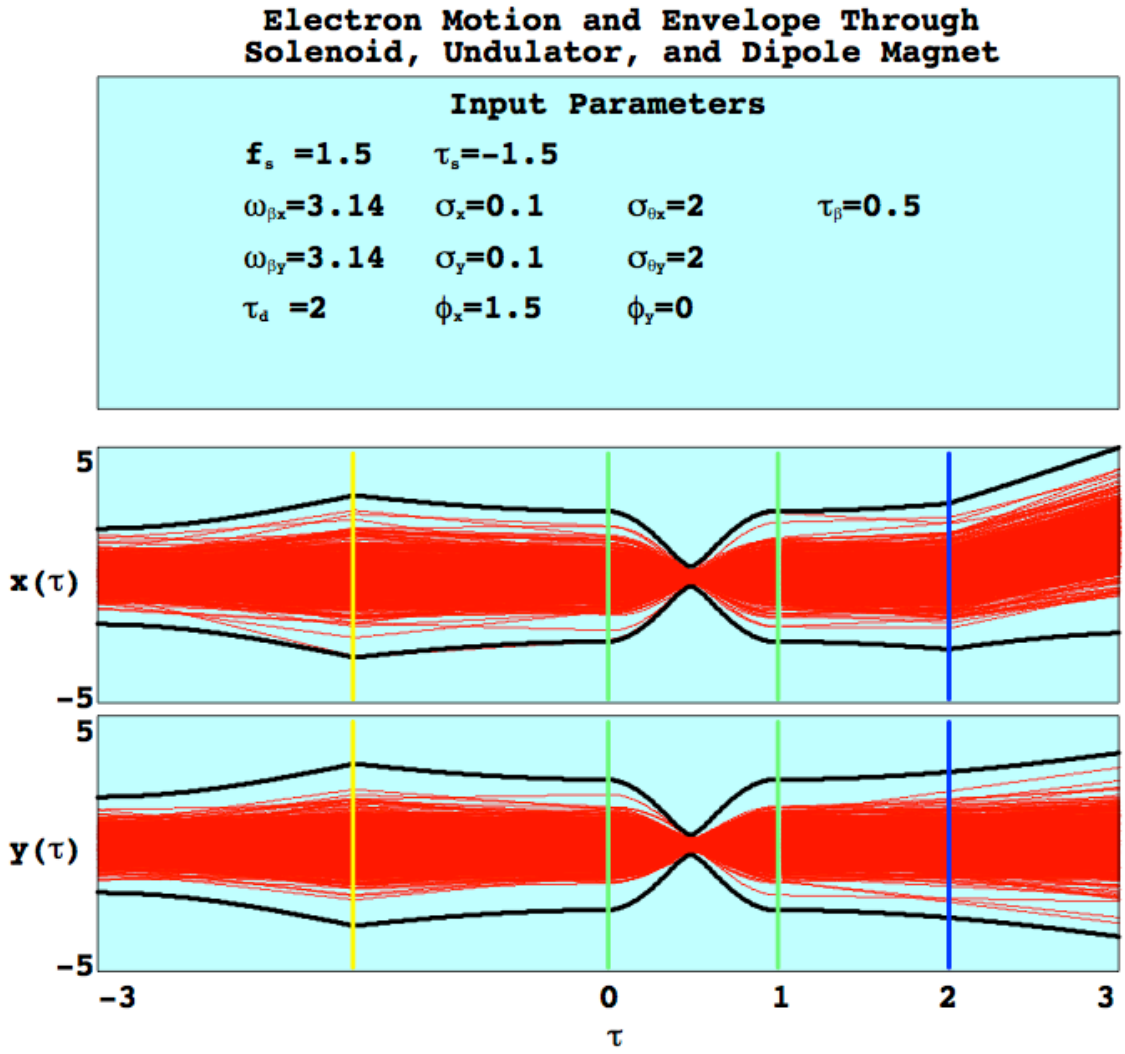

Figure 23. An output of the *solebetadipole-env.c* program. 500 sample electrons propagate through a solenoid, an undulator, and a dipole magnet, including the beam envelope. The simulation depicts that the electron trajectories are focused both in x and y by the solenoid lens.

E. GENERAL PARTICLE TRACER SIMULATION

General Particle Tracer (GPT) [13,14] is a well-developed computational tool to track charged particles through electromagnetic fields in 2D and 3D, taking space-charge effects into account. A fifth order Runge-Kutta method, with adaptive stepsize control, is used in GPT to solve the particle equations of motion. GPT requires an input file to specify the initial particle distribution, construct electromagnetic field configurations, and define the output methods. GPT includes many common beamline elements for basic

structures such as dipoles, quadrupoles, solenoids, and undulators. Because of its adaptabilities and capabilities, GPT is widely used to study beam dynamics and design beamlines for particle accelerators.

In order to compare with electron trajectories in Figures 21 and 23, I used several GPT elements and ran two simulations. The first GPT simulation modeled electron trajectories traveling along the z axis through a quadrupole triplet, an undulator and a dipole magnet. By substituting a solenoid for the quadrupoles, the second GPT simulation modeled electron trajectories through a solenoid lens, an undulator and a dipole magnet.

1. Quadrupole, Undulator, and Dipole Magnet

The first GPT simulation consists of 12 elements in the input file, **Setparticles**, **Setrxydist**, **Setphidist**, **SetGdist**, **Setgbxdist**, **Setgbydist**, **Setgbxemittance, Setgbyemittance**, **Quadrupole**, **Unduplan**, **Rectmagnet**, and **Tout**. The first eight elements determine the number of sample electrons, initial electron distributions, and electron emittances (i.e., angular spread). The initial electron transverse distribution in the first simulation is set to be a Gaussian distribution in the x and y directions with emittance. The **Quadrupole** element defines a quadrupole lens without fringe fields. The orientations of three quadrupole lenses are positioned perpendicular to the electron beam path. The **Unduplan** element defines a linear undulator. The **Rectmagnet** element models a planar rectangular magnet with optional fringe fields. The orientation of the planar rectangular magnet is in the xz plane with uniform magnetic field in the positive y direction if this element is configured to have no fringe fields. Time output intervals can be specified using the **Tout** element. The input values of betatron frequency and number of sample electrons are the same as shown in Figure 21. For the other input values in this simulation, we chose the total number of undulator periods (Nu=20) and undulator period (lamu=0.05m) first, so that the total undulator length is 1m. Then by applying the definitions in Chapter II and specified values in Figure 21, the input values of undulator field amplitude, magnetic field gradients of the quadrupoles, and magnetic field of the dipole magnetic can be determined algebraically. The main input parameters and values of the first simulation are given in Table 1.

Parameter	Description	Value	
gamma	Lorentz factor	3	
nps	Number of electrons	500	
radius	Electron beam radius	3×10^{-4}	
setgbxemittance	Requested emittance in $x\beta x$-space [m-rad]	2×10^{-8}	
setgbyemittance	Requested emittance in $y\beta y$-space [m-rad]	2×10^{-8}	
Lq	Length of the quadrupoles [m]	first	0.03
		second	0.03
		third	0.03
G	Magnetic field gradients of the quadrupoles [T/m]	first	0.285
		second	-0.57
		third	0.285
Nu	Total number of undulator periods	20	
lamu	Undulator period [m]	0.05	
Bu	Undulator field amplitude [T]	0.0228	
Bfield	Rectmagnet maximum magnetic field [T]	5×10^{-6}	
a	Length of magnet in x direction [m]	0.4	
b	Length of magnet in z direction [m]	0.4	

Table 1. Main parameters in the first GPT simulation.

Figure 24 displays a simulation of the 500 sample electron trajectories propagating at $z=-3\text{m}\rightarrow 3\text{m}$ through a quadrupole triplet, an undulator and a dipole magnet. The positions of the three quadrupoles are shown as vertical purple lines. The first and third quadrupoles are placed at $z=-1.6\text{m}$ and -1.4m with equal focal length 0.6m. The second quadrupole is placed at $z=-1.5\text{m}$ with focal length -0.3m. Electron

trajectories defocus in the x direction and focus in the y direction while passing through the first and third quadrupoles, and have reverse focusing and defocusing while passing through the second quadrupole. The position of the undulator is from $z = 0 \to 1\text{m},$ shown by vertical green lines. Electrons perform one half betatron oscillations over the length of the undulator and are focused at $z = 0.5\text{m},$ confirming that the betatron frequency is $\pi.$ The dipole magnet is placed at $z = 2\text{m},$ shown by the vertical blue line. Simulation output indicates that the electron beam is deflected in the positive x direction and undeflected in the y direction after passing through the dipole magnet. From Equations (2.70) and given values in Table 1, the theoretical bending angle of the electron beam in this simulation is calculated to be 0.01 degrees. The measured bending angle of the electron beam is 0.01 degrees. Both bending angles are so small that I conducted additional simulations by only changing input values of the dipole magnet field in Table 1 to verify the reliability of this simulation model for predicting the deflection angle. The results are listed in Table 2 from which all the measured angles are in good agreement with the theoretical bending angles. The overall electron beam paths in Figures 21 and 24 are consistent with each other.

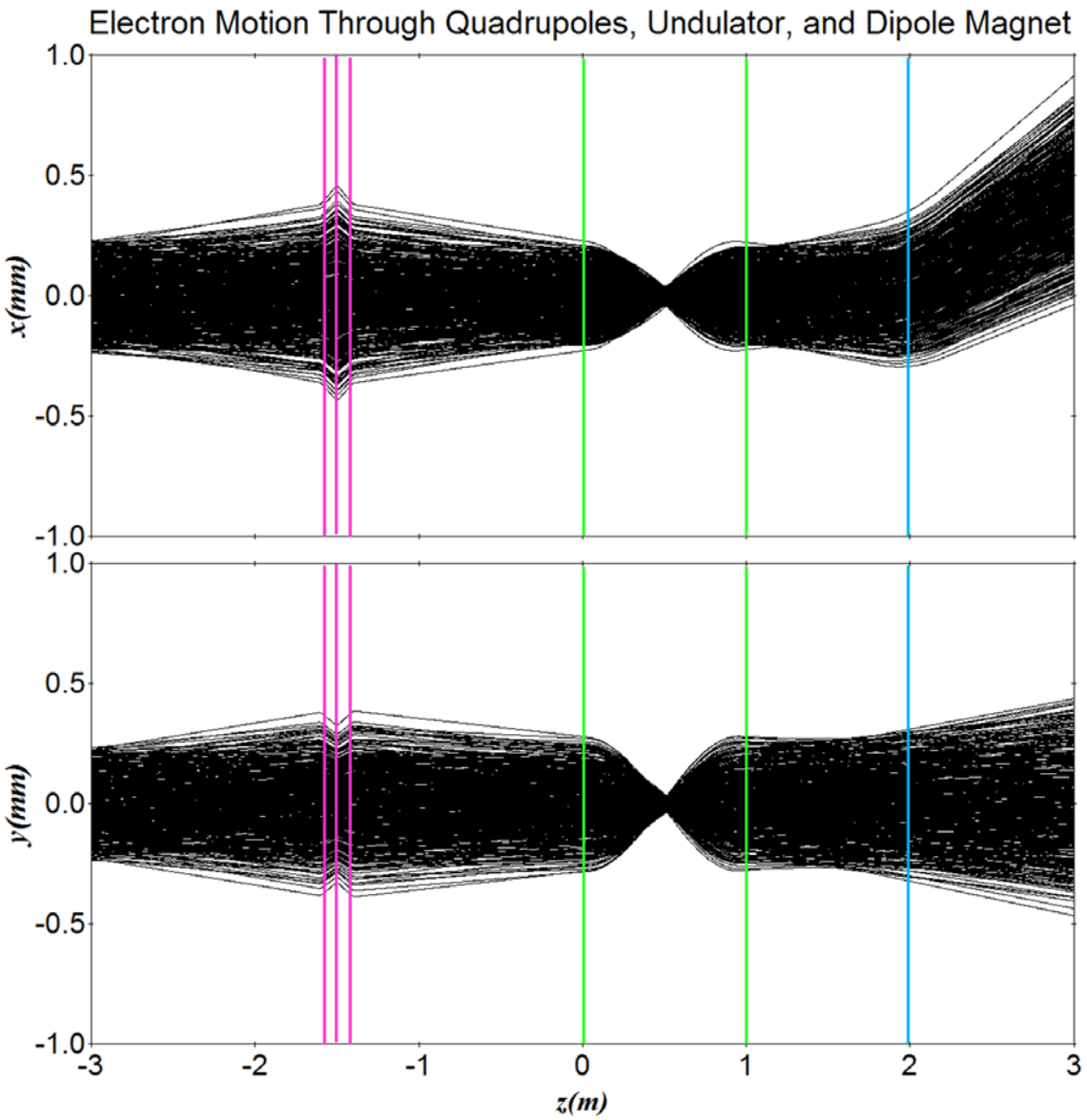

Figure 24. GPT simulation of electron beam trajectories through a quadrupole triplet, an undulator, and a dipole magnet, with the vertical axis in millimeters and horizontal axis in meters. The electron beam is focused in both x and y directions after traveling through the quadrupoles (purple lines). Betatron oscillations of the electrons occur in the undulator (green lines). The dipole magnet (blue line) causes the electron beam to deflect in the positive x direction but not in the y direction.

Rectmagnet maximum magnetic field value [T]	Theoretical bending angle [deg]	Measured bending angle [deg]
8.51×10^{-3}	45.0	44.9
7.74×10^{-3}	40.0	39.9
6.02×10^{-3}	30.0	30.0
4.12×10^{-3}	20.0	20.0
2.09×10^{-3}	10.0	10.0

Table 2. The comparison of the theoretical bending angles and measured angles by using five values of the magnetic field of the dipole magnet. The measured angles are close to the theoretical deflection angles.

2. Solenoid, Undulator, and Dipole Magnet

The second GPT program is designed to simulate electron trajectories through a solenoid lens, an undulator and a dipole magnet. The simulation program also includes twelve elements in the input file, **Setparticles**, **Setrxydist**, **Setphidist**, **SetGdist**, **Setgbxdist**, **Setgbydist**, **Setgbxemittance, Setgbyemittance**, **Bzsolenoid**, **Unduplan**, **Rectmagnet**, and **Tout**. Among these 12 elements, the functions of eleven elements have been introduced in last section. The **Bzsolenoid** element is used to model a solenoid lens. The orientation of the loop is positioned perpendicular to the electron beam path with the beam going through its center. The values of betatron frequency and number of sample electrons are the same as in Figure 23. The input values of undulator field amplitude, current of the solenoid, and magnetic field of the dipole magnetic are specified by using the definitions in Chapter II and values in Figure 23. The main input parameters and values of this simulation are given in Table 3. The fringe field for the rectangular magnet is excluded in this simulation as well.

Parameter	Description	Value
gamma	Lorentz factor	3
nps	Number of electrons	500
radius	Electron beam radius	3×10^{-4}
setgbxemittance	Requested emittance in $x\beta x$-space [m-rad]	2×10^{-8}
setgbyemittance	Requested emittance in $y\beta y$-space [m-rad]	2×10^{-8}
R	Radius of solenoid [m]	0.02
Ls	Solenoid length [m]	0.065
nI	Ampere turns per meter [A]	30770
Nu	Total number of undulator periods	20
lamu	Undulator period [m]	0.05
Bu	Undulator field amplitude [T]	0.0228
Bfield	Rectmagnet maximum magnetic field [T]	5×10^{-6}
a	Length of magnet in x direction [m]	0.4
b	Length of magnet in z direction [m]	0.4

Table 3. Main parameters in the second simulation.

Figure 25 depicts electron beam paths through a solenoid lens, an undulator, and a dipole magnet. The position of the solenoid lens with focal length 1.5m is located at $z=-1.5\text{m}$ (yellow line). The plot shows that the electron beam is converged in both x and y direction simultaneously after passing through the solenoid lens. Then electrons undergo betatron motion in the undulator region (green lines) and focus in the middle of the undulator. Electrons complete one half betatron oscillation confirming that the betatron frequency is π. The blue line indicates the position of the dipole magnet ($z=2\text{m}$) at which the electron beam is deflected in the positive x direction but not in the y direction. The measured bending angle of the electron beam is 0.01 degrees from

other simulation output (not shown), which is the same as the theoretical bending angle. The simulation result of electron beam in Figure 25 is in excellent agreement with the previous result in Figure 23.

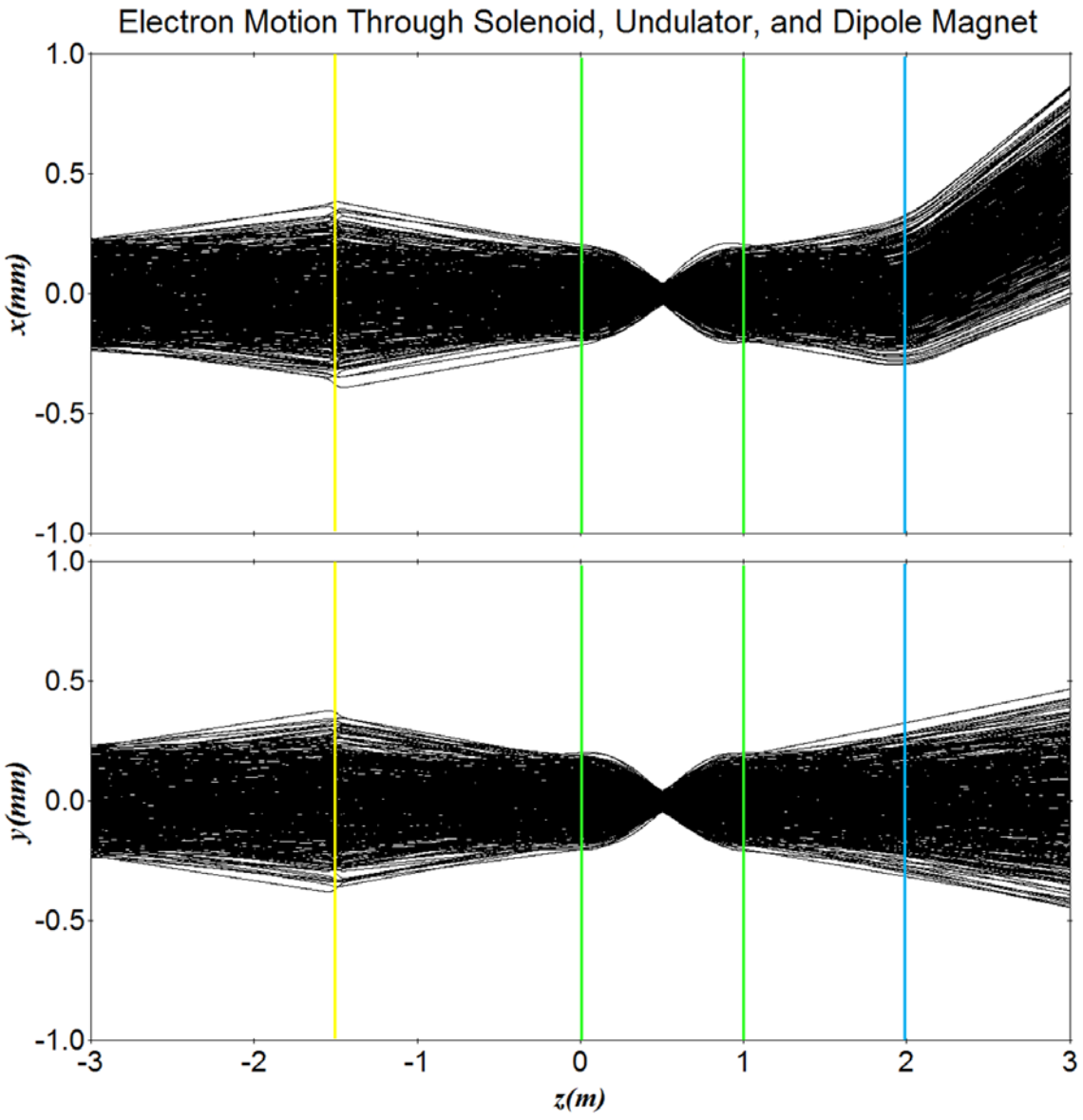

Figure 25. A plot of electron beam trajectories through a solenoid lens, an undulator and a dipole magnet with the vertical axis in millimeters and the horizontal axis in meters. The electron paths in xz and yz are focused after passing through the solenoid lens at $z = -1.5\text{m}$. Electrons perform betatron oscillations in the undulator from $z = 0 \rightarrow 1\text{m}$. The dipole magnet located at $z = 2\text{m}$ causes the electron beam to deflect only in the positive x direction.

THIS PAGE INTENTIONALLY LEFT BLANK

IV. CONCLUSION

This thesis has discussed electron dynamics in major FEL components used for transporting and focusing of the electron beam and have developed new computational tools to simulate electron paths and the beam envelope through those components. Results from the new programs were compared to GPT, a well-established particle tracing program, and good agreement was found. Simulations demonstrated how electrons experience betatron motion in an undulator and how a quadrupole doublet or triplet provides net transverse focusing for electrons. A solenoid will focus electrons azimuthally due to the axisymmetric magnetic field, and is typically used for focusing a low energy electron beam ($<$ few MeV). Simulation plots indicate both devices focus electrons effectively, which help electrons inject into the undulator nearly collimated and then focus in the center of the undulator. Other outputs show that dipole magnets can be used to bend the electron beam, and the measured deflection angles of the electron beam agree with a theoretical formula. This study will help improve the design of beamlines for FELs. Future work could continue by including fringe effects for quadrupoles, undulators, and dipole magnets, and considering the effects of misalignment of these elements.

THIS PAGE INTENTIONALLY LEFT BLANK

LIST OF REFERENCES

[1] A. E. Siegman, *Lasers*, 1st ed. Herndon, VA: University Science Books, 1986.

[2] W. B. Colson, "Electric ship weapon systems," class notes for PH4858, Department of Physics, Naval Postgraduate School, Monterey, CA, Fall 2012.

[3] J. Blau, "Free electron laser physics," class notes for PH4055, Department of Physics, Naval Postgraduate School, Monterey, CA, Summer 2013.

[4] Jefferson Labs, "Thomas Jefferson National Accelerator Facility." [Online]. Available: http://www.flickr.com/photos/jeffersonlab/ [Accessed: August 15, 2013].

[5] "Undulator." [Online]. In *Wikipedia*. Available: http://en.wikipedia.org/wiki/Undulator [Accessed: August 8, 2013].

[6] M. Reiser, *Theory and Design of Charged Particle Beams*, 2nd ed. Weinheim, Germany: Wiley-VCH, 2008.

[7] National KR Tech, "Quadrupole magnet." [Online]. Available: http://www.krtech.co.kr/ [Accessed: February 24, 2013].

[8] National Synchrotron Radiation Research Center. [Online]. Available: http://www.nsrrc.org.tw/ [Accessed: February 25, 2013].

[9] Physics Stack Exchange. [Online]. Available: http://physics.stackexchange.com/questions/38067/magnetic-field-lines-can-be-entirely-confined-within-the-core-of-a-toroid-but-n [Accessed: October 10, 2013].

[10] D. J. Griffiths, *Introduction to Electrodynamics*, 3rd ed. Boston: Addison Wesley, 1999.

[11] S. Humphries, Jr., *Principles of Charged Particle Acceleration*, 1st ed. New York: Dover Publications, 2012.

[12] A.S. Laney, "The Effects of Accelerator Frequency and Electron Beam Focusing in Free Electron Lasers," M.S. thesis, Physics Department, Naval Postgraduate School, 2012.

[13] S.B. van der Geer, and M.J. de Loos, "General Particle Tracer: A 3D Code for Accelerator and Beamline Design," *Proc. 1998 Particle Accel. Conf.*, Stockholm, Sweden (1998), pp. 1245.

[14] GPT User Manual, Pulsar Physics, De Bongerd 23, 3762 XA Soest, The Netherlands. [Online]. Available: http://www.pulsar.nl/gpt.

THIS PAGE INTENTIONALLY LEFT BLANK

INITIAL DISTRIBUTION LIST

1. Defense Technical Information Center
   Ft. Belvoir, VA

2. Dudley Knox Library
   Naval Postgraduate School
   Monterey, CA